POLITECNICO DI TORINO
Repository ISTITUZIONALE

Finite volume form factors in the presence of integrable defects

Terms of use:

Publisher copyright

(Article begins on next page)

28 April 2024

Finite volume form factors in the presence of integrable defects

Z. Bajnok [a,*], F. Buccheri [b], L. Hollo [a], J. Konczer [a], G. Takacs [b,c]

[a] *MTA Lendület Holographic QFT Group, Wigner Research Centre for Physics, H-1525 Budapest 114,*
P.O. Box 49, Hungary
[b] *MTA-BME "Momentum" Statistical Field Theory Research Group, Budafoki út 8,*
1111 Budapest, Hungary
[c] *Department of Theoretical Physics, Budapest University of Technology and Economics, Budafoki út 8,*
1111 Budapest, Hungary

Received 7 February 2014; accepted 17 March 2014

Available online 21 March 2014

Editor: Hubert Saleur

Abstract

We developed the theory of finite volume form factors in the presence of integrable defects. These finite volume form factors are expressed in terms of the infinite volume form factors and the finite volume density of states and incorporate all polynomial corrections in the inverse of the volume. We tested our results, in the defect Lee–Yang model, against numerical data obtained by truncated conformal space approach (TCSA), which we improved by renormalization group methods adopted to the defect case. To perform these checks we determined the infinite volume defect form factors in the Lee–Yang model exactly, including their vacuum expectation values. We used these data to calculate the two point functions, which we compared, at short distance, to defect CFT. We also derived explicit expressions for the exact finite volume one point functions, which we checked numerically. In all of these comparisons excellent agreement was found.

1. Introduction

The complete solution of a quantum field theory means the determination of its spectrum and correlation functions. This ultimate goal is almost impossible to achieve in general dimensions

---

and for generic interacting theories. However, in two-dimensional integrable models even such an ambitious plan can be fulfilled.

For many quantities, such as operator matrix elements, a numerical determination is only possible in finite volumes [20]. Such determination can be performed using the tools of lattice field theory or, in the case of two-dimensional quantum field theories, a more specialized method such as the truncated conformal space approach (TCSA) [28]. Finite volume quantities are also interesting on their own right in statistical field theory, as well as in particle physics. The general strategy to compute them analytically is to solve the theory in infinite volume first and then to take into account the finite size corrections systematically. The infinite volume solution is carried out in the bootstrap framework, and it consists of the scattering matrix bootstrap and the form factor bootstrap parts. All finite size corrections can be expressed purely in terms of these infinite volume characteristics of the theory in a framework that was pioneered by Lüscher [17–19].

The infinite volume solution of an integrable QFT starts with the S-matrix bootstrap. The scattering matrix satisfies unitarity and crossing symmetry and all of its poles are located on the imaginary rapidity axes and correspond to bound-states or some Coleman–Thun type diagrams. Assuming one single particle in the spectrum with a self-fusing pole the bootstrap leads to the S-matrix of the scaling Lee–Yang model. Introducing integrable boundaries or integrable defects requires additionally to perform this bootstrap program for the reflection and transmission matrices. The structure of the scattering, reflection and transmission matrices contain all information about the infinite volume spectrum of bulk, boundary or defect excitations. Once this first bootstrap step is completed, the resulting scattering, reflection and transmission matrices can be used to formulate consistency requirements for the matrix elements of local operators between asymptotic states (form factors). Solutions to these requirements compatible with the analytical structure demanded by physics lead to the determination of the form factors of all local bulk, boundary and defect operators. These form factors then can be used to build up all correlation functions in infinite volume.

Once all infinite volume characteristics are determined they can be used to decrease the volume gradually and continue the quantities for finite volumes. The leading volume dependence is polynomial in the inverse of the volume, while the sub-leading ones are exponentially small. The polynomial finite size corrections for the spectrum can be formulated in terms of the scattering, reflection or transmission matrices. At this order the dispersion relation is not changed, but the energy levels are quantized. Momentum is quantized in a finite volume as, if we move a particle around the 1D 'world', we collect not only the translational phase, but also the phases of all scatterings and/or reflections and transmissions: therefore, imposing periodic boundary conditions restricts the allowed particle momenta. The resulting equations are called Bethe–Yang equations. Exponentially small corrections are due to vacuum polarization effects and can be taken into account by the Thermodynamic Bethe Ansatz method.

Finite volume form factors are the matrix elements of local operators between the finite volume eigenstates of the Hamiltonian. Just like for the spectrum, leading finite size corrections are polynomial in the inverse of the volume, while sub-leading corrections are exponentially small. The polynomial corrections are related to the normalization of the Bethe–Yang eigenvectors and were systematically analyzed in [23,24] for periodic boundary conditions, while in [16] for general integrable boundary conditions. The aim of the present paper is to generalize this analysis for the defect case. We mention for completeness that the exponential finite size corrections have not been described yet, except for some recent results accounting for the composite structure of bound states [21,27], and for diagonal form factors in the case of periodic boundary conditions [22].

Integrable interacting defects are either purely reflective (i.e. boundaries) or purely trans-missive [10]. Recently there was relevant progress in identifying and solving purely transmitting defect theories [6–8,1,11]. In this paper we focus on the simplest integrable defect theory, namely the defect Lee–Yang model. The T-matrix bootstrap of this model was performed in [3], while the form factor bootstrap program was initiated in [4].

Our paper is organized as follows: In Section 2, we recall the infinite volume form factor so-lution of the defect Lee–Yang model. We start by listing the defect form factor axioms. We then introduce the defect Lee–Yang model both from the scattering (IR) and from the perturbed CFT (UV) side. In presenting the defect form factors we go beyond the results available in the litera-ture, as we determine all form factor solutions of primary fields. Technical details are relegated to Appendix A. In order to have properly normalized form factors, we calculate the vacuum ex-pectation values of all primary fields. The form factors and normalizations are checked against the defect CFT two point functions. In Section 3 we develop the leading finite size corrections of defect form factors. We analyze separately the non-diagonal and diagonal cases as in the lat-ter one disconnected terms appear which have to be determined carefully. Section 4 contains the checks of our results against the numerically "measured" finite volume matrix elements cal-culated by the defect TCSA (DTCSA) method. In Section 5 we derive the exact finite volume vacuum expectation values of local fields what we also check numerically. Finally we draw our conclusions in Section 6.

2. Form factors in infinite volume

In this section we recall the theory of form factors in the presence of integrable defects fol-lowing [4]. We focus on a relativistic integrable theory which contains one particle type only. Energy and momentum of the particles are parametrized by the rapidity variable θ:

$$E(\theta) = m \cosh \theta, \qquad p(\theta) = m \sinh \theta \tag{1}$$

and Lorentz transformation simply shifts the rapidity: $\theta \to \theta + \Lambda$. Integrability forces the multi-particle scattering matrix to factorize into pairwise two particle scatterings, which depends on the rapidity differences $S(\theta_1 - \theta_2)$ and satisfies unitarity and crossing symmetry

$$S(\theta) = S(-\theta)^{-1}; \qquad S(i\pi - \theta) = S(\theta). \tag{2}$$

If the S-matrix has a pole at $\theta = i\frac{2\pi}{3}$ (like in the scaling Lee–Yang model) then it has to satisfy the fusion equation

$$S(\theta)|_{\theta \approx i\frac{2\pi}{3}} = -i\frac{\Gamma^2}{\theta - i\frac{2\pi}{3}} + \text{reg. terms} \longrightarrow S(\theta) = S\left(\theta - i\frac{\pi}{3}\right)S\left(\theta + i\frac{\pi}{3}\right), \tag{3}$$

which shows that the particle is a bound-state of itself.

Introducing an integrable defect means that we cut the space–time into two halves and as-sociate an amplitude of crossing through the defect. Particles coming from the left cross with $T_-(\theta)$, while those coming from the right cross with $T_+(-\theta)$. The T_+ transmission factor is parametrized such that for its physical domain of rapidities ($\theta < 0$) its argument is always posi-tive. Unitarity and crossing symmetry relates these two amplitudes as [2]:

$$T_-(\theta) = T_+(-\theta)^{-1}; \qquad T_-(\theta) = T_+(i\pi - \theta) \tag{4}$$

A prototype of a parity symmetric defect is a standing particle with $T_-(\theta) = S(\theta) = T_+(\theta)$. A non-parity symmetric defect can be realized as an imaginary rapidity "bound" particle:

$T_{\pm}(\theta) = S(\theta \pm iu)$. In the case of a fusion pole, (3), the defect satisfies the fusion equation as well:

$$T_-(\theta) = T_-\left(\theta - i\frac{\pi}{3}\right) T_-\left(\theta + i\frac{\pi}{3}\right) \tag{5}$$

and likewise for T_+. It might happen that the transmission factor exhibits a pole

$$T_-(\theta)|_{\theta \approx iv} = -i\frac{g^2}{\theta - iv} + \text{reg. terms} \tag{6}$$

signaling a defect bound-state.

Integrable defects are topological in the sense that the location of the defect can be changed without altering the amplitude of any multi-particle transmission process unless it crosses an insertion point of any field. As a consequence multi-particle transmissions factorize into the product of pairwise scatterings and individual transmissions.

In the following we recall the form factor axioms in the presence of these integrable defects [4].

2.1. Summary of the defect form factor bootstrap

Form factors are the matrix elements of local operators between asymptotic states:

$$\langle \theta'_{m'+n'}, \ldots, \theta'_{n'+1}; \theta'_{n'}, \ldots, \theta'_1 | \mathcal{O}(x,t) | \theta_1, \ldots, \theta_n; \theta_{n+1}, \ldots, \theta_{n+m} \rangle \tag{7}$$

where in the presence of defects we have to distinguish if particles arrive from the left or from the right. In an initial state the rapidities are ordered as

$$\theta_1 > \cdots > \theta_n > 0 > \theta_{n+1} > \cdots > \theta_{n+m} \tag{8}$$

while in the final state oppositely $\theta'_{m'+n'} > \cdots > \theta'_{n'+1} > 0 > \theta'_{n'} > \cdots > \theta'_1$. The form factor is originally defined for initial and final states and then analytically continued for any orderings of its arguments. Interestingly, the presence of an integrable defect breaks the translation invariance by having non-zero momentum (like a bound particle) and not by destroying the existence of the momentum itself. As a consequence the space–time dependence of the form factor is

$$\langle \theta'_{m'+n'}, \ldots, \theta'_{n'+1}; \theta'_{n'}, \ldots, \theta'_1 | \mathcal{O}(x,t) | \theta_1, \ldots, \theta_n; \theta_{n+1}, \ldots, \theta_{n+m} \rangle$$
$$= e^{it\Delta E - ix\Delta P} F^{\mathcal{O}_{\pm}}_{(n',m')(n,m)}\left(\theta'_{n'+m'}, \ldots, \theta'_{n'+1}; \theta'_{n'}, \ldots, \theta'_1 | \theta_1, \ldots, \theta_n; \theta_{n+1}, \ldots, \theta_{n+m}\right) \tag{9}$$

with $\Delta E = m(\sum_j \cosh\theta_j - \sum_{j'} \cosh\theta'_{j'})$ and $\Delta P = m(\sum_j \sinh\theta_j - \sum_{j'} \sinh\theta'_{j'})$, and we distinguished if the operator was localized on the left, $\mathcal{O}_-$, or on the right, $\mathcal{O}_+$, of the defect as they might not be continuous there. Same apply for operators localized at the defect ($x = 0$). Crossing transformation of any of the form factors

$$F^{\mathcal{O}}_{(n',m')(n,m)}\left(\theta'_{n'+m'}, \ldots, \theta'_{n'+1}; \theta'_{n'}, \ldots, \theta'_1 | \theta_1, \ldots, \theta_n; \theta_{n+1}, \ldots, \theta_{n+m}\right)$$
$$= F^{\mathcal{O}}_{(n',m'+1)(n,m-1)}\left(\theta_{n+m} + i\pi, \theta'_{n'+m'}, \ldots, \theta'_{n'+1}; \theta'_{n'}, \ldots, \theta'_1 | \theta_1, \ldots, \theta_n; \theta_{n+1}, \ldots, \theta_{n+m-1}\right) \tag{10}$$

$$F^{\mathcal{O}}_{(n',m')(n,m)}\left(\theta'_{n'+m'}, \ldots, \theta'_{n'+1}; \theta'_{n'}, \ldots, \theta'_1 | \theta_1, \ldots, \theta_n; \theta_{n+1}, \ldots, \theta_{n+m}\right)$$
$$= F^{\mathcal{O}}_{(n'+1,m')(n-1,m)}\left(\theta'_{n'+m'}, \ldots, \theta'_{n'+1}; \theta'_{n'}, \ldots, \theta'_1, \theta_1 - i\pi | \theta_2, \ldots, \theta_n; \theta_{n+1}, \ldots, \theta_{n+m}\right) \tag{11}$$

can be used to bring all particles into one side:

$$F_{(n,m)}^{\mathcal{O}}(\theta_1,\ldots,\theta_n;\theta_{n+1},\ldots,\theta_{n+m}) := F_{(0,0)(n,m)}^{\mathcal{O}}(;|\theta_1,\ldots,\theta_n;\theta_{n+1},\ldots,\theta_{n+m}) \tag{12}$$

We can also use transmission

$$\begin{aligned}
&F_{(n,m)}^{\mathcal{O}}(\theta_1,\ldots,\theta_n;\theta_{n+1},\ldots,\theta_{n+m}) \\
&= T_-(\theta_n) F_{(n-1,m+1)}^{\mathcal{O}}(\theta_1,\ldots,\theta_{n-1};\theta_n,\theta_{n+1},\ldots,\theta_{n+m})
\end{aligned} \tag{13}$$

to define the *elementary* form factors

$$F_n^{\mathcal{O}}(\theta_1,\ldots,\theta_n) = F_{(n,0)}^{\mathcal{O}}(\theta_1,\ldots,\theta_n;) \tag{14}$$

which satisfies the axioms

$$F_n^{\mathcal{O}}(\theta_1,\ldots,\theta_i,\theta_{i+1},\ldots,\theta_n) = S(\theta_i - \theta_{i+1}) F_n^{\mathcal{O}}(\theta_1,\ldots,\theta_{i+1},\theta_i,\ldots,\theta_n) \tag{15}$$

$$F_n^{\mathcal{O}}(\theta_1,\theta_2,\ldots,\theta_n) = F_n^{\mathcal{O}}(\theta_2,\ldots,\theta_n,\ldots,\theta_1 - 2i\pi) \tag{16}$$

$$-i\operatorname{Res}_{\theta=\theta'} F_{n+2}^{\mathcal{O}}(\theta+i\pi,\theta',\theta_1,\ldots,\theta_n) = \left(1 - \prod_{j=1}^{n} S(\theta-\theta_j)\right) F_n^{\mathcal{O}}(\theta_1,\ldots,\theta_n) \tag{17}$$

$$-i\operatorname{Res}_{\theta=\theta'} F_{n+2}^{\mathcal{O}}\left(\theta+\frac{i\pi}{3},\theta'-\frac{i\pi}{3},\theta_1,\ldots,\theta_n\right) = \Gamma F_{n+1}^{\mathcal{O}}(\theta,\theta_1,\ldots,\theta_n) \tag{18}$$

$$-i\operatorname{Res}_{\theta=iu} F_{n+1}^{\mathcal{O}}(\theta_1,\ldots,\theta_n,\theta) = ig\tilde{F}_n^{\mathcal{O}}(\theta_1,\ldots,\theta_n) \tag{19}$$

where $\tilde{F}$ is the form factor on the excited defect state. Although the axioms (15)–(18) look the same as the form factor axioms without the defect they are valid only for particles coming from the left (see Eq. (14)). For any particle coming from the right one has to include a transmission factor, see Eq. (13).

The form factor of a bulk operator localized on the left of the defect, $\mathcal{O}_-$, is simply its bulk form factor

$$F_n^{\mathcal{O}_-}(\theta_1,\ldots,\theta_n) = B_n^{\mathcal{O}}(\theta_1,\ldots,\theta_n) \tag{20}$$

but when the same operator is localized on the right of the defect, $\mathcal{O}_+$, its form factor is

$$F_n^{\mathcal{O}_+}(\theta_1,\ldots,\theta_n) = \prod_i T_-(\theta_i) B_n^{\mathcal{O}}(\theta_1,\ldots,\theta_n) \tag{21}$$

These apply for the left/right limits of the bulk fields at the defect as well.

As we assume that the bulk form factors are already determined in [30] we focus on form factors of defect operators. In general, the solution compatible with the form factor axioms takes the form

$$F_n^{\mathcal{O}}(\theta_1,\ldots,\theta_n) = \langle\mathcal{O}\rangle H_n \prod_i d(\theta_i) \prod_{i<j} \frac{f(\theta_i-\theta_j)}{x_i+x_j} Q_n(x_1,\ldots,x_n) \tag{22}$$

where $f(\theta)$ is the minimal bulk two particle form factor, which satisfies:

$$f(\theta) = S(\theta)f(-\theta); \qquad f(i\pi-\theta) = f(i\pi+\theta) \tag{23}$$

The one particle minimal defect form factor $d(\theta)$ is responsible for defect bound-states, H_n is some normalization constant and Q_n is a symmetric polynomial in its arguments $x_i = e^{\theta_i}$.

2.2. Defect form factors in the scaling Lee–Yang model

The Lee–Yang model is the simplest conformal field theory, the $\mathcal{M}_{2,5}$ minimal model, whose central charge is $c = -\frac{22}{5}$ and which has only two irreducible Virasoro representations V_0 and V_h with highest weights 0 and $h = -\frac{1}{5}$, respectively. The periodic Lee–Yang model carries a representation of $Vir \otimes \overline{Vir}$ and its Hilbert-space is decomposed as

$$\mathcal{H} = V_0 \otimes \bar{V}_0 + V_h \otimes \bar{V}_h \tag{24}$$

We can associate a local field for all vector of the Hilbert-space, and for the highest weight states these fields are the identity $\mathbb{I}$ and Φ, respectively. These local fields form an operator-algebra with the operator product expansions

$$\Phi(z, \bar{z})\Phi(0, 0) = C_{\Phi\Phi}^{\mathbb{I}} |z|^{-4h} \mathbb{I} + C_{\Phi\Phi}^{\Phi} |z|^{-2h} \Phi(0, 0) + \cdots \tag{25}$$

In order to have a real field $\Phi^\dagger = \Phi$, we normalized the field as $C_{\Phi\Phi}^{\mathbb{I}} = -1$. A consistent choice of the other structure constant is $C_{\Phi\Phi}^{\Phi} = \sqrt{\frac{2}{1+\sqrt{5}} \frac{\Gamma(\frac{1}{5})\Gamma(\frac{6}{5})}{\Gamma(\frac{3}{5})\Gamma(\frac{4}{5})}} \approx 1.91131\ldots$

In this subsection we specify the previous defect form factor considerations for the scaling Lee–Yang model [3]. The scaling Lee–Yang model is the single relevant perturbation of the Lee–Yang model

$$\mathcal{A} = \mathcal{A}_{LY} - \lambda \int d^2z \, \Phi(z, \bar{z}) \tag{26}$$

and has a single particle in the spectrum with the two-particle scattering matrix:

$$S(\theta) = \frac{\sinh\theta + i \sin\frac{\pi}{3}}{\sinh\theta - i \sin\frac{\pi}{3}} \tag{27}$$

There is a one parameter family of integrable defect perturbation of the defect Lee–Yang model [5] which has the transmission factor

$$T_\pm(\theta) = S\left(\theta \pm i\frac{\pi}{6}(3 - b)\right) \tag{28}$$

Formally it is like a particle with rapidity $\theta = i\frac{\pi}{6}(3 - b)$ and the defect energy and momentum are indeed

$$e_d = m \sin\frac{\pi b}{6}; \qquad p_d = im \cos\frac{\pi b}{6} \tag{29}$$

This theory can be realized as a unique one parameter family of integrable perturbation of the defect Lee–Yang model:

$$S^d = S_{LY}^d - \lambda \int d^2z \, \Phi(z, \bar{z}) - \mu \int dy \, \varphi(y) - \bar{\mu} \int dy \, \bar{\varphi}(y) \tag{30}$$

where integrability forces the constraint:

$$\lambda = \mu\bar{\mu}\xi^{-2}; \quad \xi^{-2} = 2i\sqrt{\frac{1+\sqrt{5}}{2}} \frac{1 - e^{i\pi/5}}{1 + e^{i\pi/5}} = 0.826608 \tag{31}$$

The relation between the Lagrangian and scattering parameters is

$$\lambda = \left(\frac{m}{\kappa}\right)^{\frac{12}{5}}; \quad \kappa = 2^{\frac{19}{12}}\sqrt{\pi}\frac{(\Gamma(\frac{3}{5})\Gamma(\frac{4}{5}))^{\frac{5}{12}}}{5^{\frac{5}{16}}\Gamma(\frac{2}{3})\Gamma(\frac{5}{6})} = 2.642944 \tag{32}$$

$$\mu = \left(\frac{m}{\kappa}\right)^{\frac{6}{5}}\xi e^{-\frac{i\pi}{5}(3+b)}; \qquad \bar{\mu} = \left(\frac{m}{\kappa}\right)^{\frac{6}{5}}\xi e^{\frac{i\pi}{5}(3+b)} \tag{33}$$

Due to the nontrivial defect, the Hilbert space of the defect Lee–Yang model

$$\mathcal{H} = V_0 \otimes \bar{V}_h + V_h \otimes \bar{V}_0 + V_h \otimes \bar{V}_h =: [\bar{d}] + [d] + [D] \tag{34}$$

does not coincide with the operator space localized on the defect which is

$$V_0 \otimes \bar{V}_0 + V_h \otimes \bar{V}_0 + V_0 \otimes \bar{V}_h + 2V_h \otimes \bar{V}_h =: [\mathbb{I}] + [\varphi] + [\bar{\varphi}] + [\Phi_{\pm}] \tag{35}$$

We are going to compute the form factors of these operators.

2.2.1. Form factor solutions

The ingredients of the form factor solutions are as follows: the minimal solution of the bulk two particle form factor is

$$f(\theta) = \frac{x + x^{-1} - 2}{x + x^{-1} + 1}v(i\pi - \theta)v(-i\pi + \theta), \quad x = e^{\theta} \tag{36}$$

where

$$\log v(\theta) = 2\int_0^{\infty}\frac{dt}{t}e^{\frac{i\theta t}{\pi}}\frac{\sinh\frac{t}{2}\sinh\frac{t}{3}\sinh\frac{t}{6}}{\sinh^2 t}, \tag{37}$$

which automatically includes the pole of the dynamical singularity. This minimal solution satisfies the identities

$$f(\theta)f(\theta + i\pi) = \frac{\sinh(\theta)}{\sinh(\theta) - i\sin(\frac{\pi}{3})}$$

$$f\left(\theta + \frac{i\pi}{3}\right)f\left(\theta - \frac{i\pi}{3}\right) = \frac{\cosh(\theta) + \frac{1}{2}}{\cosh(\theta) + 1}f(\theta). \tag{38}$$

The normalization factor is the same as in the bulk

$$H_n = \left(\frac{i3^{\frac{1}{4}}}{2^{\frac{1}{2}}v(0)}\right)^n. \tag{39}$$

The one particle defect form factor, which accommodates the possible defect bound-state pole is

$$d(\theta) = \frac{1}{\sqrt{3} + xv + x^{-1}\bar{v}} \tag{40}$$

where we introduced $v = e^{i\frac{\pi b}{6}}$ and $\bar{v} = v^{-1}$, satisfying

$$d(\theta + i\pi)d(\theta) = \frac{1}{1 - 2\cos(\frac{b\pi}{3} - 2i\theta)}$$

$$d\left(\theta + \frac{i\pi}{3}\right)d\left(\theta - \frac{i\pi}{3}\right) = \frac{1}{2\cos(\frac{b\pi}{6} - i\theta)}d(\theta). \tag{41}$$

Table 1
The form factor solutions of the primary fields up to level 2.

Operator	Q_1	Q_2
Φ_-	$\nu\sigma_1 + \bar{\nu}\bar{\sigma}_1 + \sqrt{3}$	$\sigma_1(\nu^2\sigma_2 + \sqrt{3}\nu\sigma_1 + \sigma_1\bar{\sigma}_1 + 1 + \sqrt{3}\bar{\nu}\bar{\sigma}_1 + \bar{\nu}^2\bar{\sigma}_2)$
Φ_+	$\nu\sigma_1 + \bar{\nu}\bar{\sigma}_1 - \sqrt{3}$	$\sigma_1(\nu^2\sigma_2 - \sqrt{3}\nu\sigma_1 + \sigma_1\bar{\sigma}_1 + 1 - \sqrt{3}\bar{\nu}\bar{\sigma}_1 + \bar{\nu}^2\bar{\sigma}_2)$
$\bar{\varphi}$	$\bar{\nu}\bar{\sigma}_1$	$\bar{\nu}\sigma_1(\bar{\nu}\bar{\sigma}_2 + \nu)$
φ	$\nu\sigma_1$	$\nu\sigma_1(\nu\sigma_2 + \bar{\nu})$

The singularity axioms provide recursion relations between the polynomials Q_n as

$$Q_{n+2}(-x, x, x_1, \ldots, x_n) = K_n(x, x_1, \ldots, x_n)Q_n(x_1, \ldots, x_n)$$
$$Q_{n+1}(x\omega, x\bar{\omega}, x_1, \ldots, x_{n-1}) = D_n(x, x_1, \ldots, x_{n-1})Q_n(x, x_1, \ldots, x_{n-1}) \qquad (42)$$

where $\omega = e^{\frac{i\pi}{3}}$, $\bar{\omega} = \omega^{-1}$ and we explicitly have

$$
\begin{aligned}
&K_n(x, x_1, \ldots, x_n) \\
&= (-1)^n\left(x^2\nu^2 - 1 + x^{-2}\nu^{-2}\right) \\
&\quad \times \frac{x}{2(\omega - \bar{\omega})}\left(\prod_{i=1}^{n}(x\omega + x_i\bar{\omega})(x\bar{\omega} - x_i\omega) - \prod_{i=1}^{n}(x\omega - x_i\bar{\omega})(x\bar{\omega} + x_i\omega)\right)
\end{aligned}
\qquad (43)
$$

for the kinematical recursion and

$$D_n(x, x_1, \ldots, x_{n-1}) = \left(\nu x + \nu^{-1}x^{-1}\right)x\prod_{i=1}^{n-1}(x + x_i) \qquad (44)$$

for the dynamical one. Since $Q_n(x_1, \ldots, x_n)$ is a symmetric polynomial we use the elementary symmetric polynomials $\sigma_k^{(n)}$, $\bar{\sigma}_k^{(n)}$, defined by the generating function:

$$\prod_{i=1}^{n}(x + x_i) = \sum_{k \in \mathbb{Z}} x^{n-k}\sigma_k^{(n)}(x_1, \ldots, x_n); \qquad \bar{\sigma}_k^{(n)}(x_1, \ldots, x_n) = \sigma_k^{(n)}\left(x_1^{-1}, \ldots, x_n^{-1}\right) \qquad (45)$$

to formulate the results. Note that $\sigma_k^{(n)} = 0$, if $k > n$ or if $k < 0$. We sometimes abbreviate $\sigma_k^{(n)}(x_1, \ldots, x_n)$ to σ_k if it does not lead to any confusion.

The form factors of the left/right limits of the bulk operator $\Phi_{\mp}$ follows from our previous considerations and are trivially related to the bulk form factors. The low lying form factors of the two chiral fields living only at the defects have been already calculated[1] [4]. The results are summarized in Table 1.

In Appendix A we explicitly derive all possible solutions of the form factor equations and extend these results to any order. Here we list only the outcome.

The form factors of the two limits of the bulk fields, $\Phi_{\pm}$, are described in terms of the bulk form factor solutions as

$$Q_n^{\Phi_\pm}(x_1, \ldots, x_n) = \prod_{i=1}^{n}\left(\nu x_i + \bar{\nu}x_i^{-1} \mp \sqrt{3}\right)\sigma_1\sigma_{n-1}P_n \qquad (46)$$

---

[1] To match with the TCSA calculation we choose a different normalization for φ and $\bar{\varphi}$ than in [4].

where

$$P_n = \det \Sigma^{(n)}, \qquad \Sigma_{ij}^{(n)} = \sigma_{3i-2j+1}^{(n)}(x_1, \ldots, x_n) \tag{47}$$

The defect form factors have the generic structure:

$$Q_n = R(\sigma_1, \bar{\sigma}_1)\sigma_n P_n S_n \tag{48}$$

where S_n does not depend on the operator:

$$S_n = \tau_{n-1} + \sum_{m \geqslant 1}(-1)^m(\tau_{n+1-6m} + \tau_{n-1-6m}); \qquad \tau_k = \sum_{l \in \mathbb{Z}} \nu^{2l-k}\bar{\sigma}_{k-l}\sigma_l, \tag{49}$$

while the operator dependent parts are

$$R^{\bar{\varphi}}(\sigma_1, \bar{\sigma}_1) = \bar{\nu}\bar{\sigma}_1; \qquad R^{\varphi}(\sigma_1, \bar{\sigma}_1) = \nu\sigma_1. \tag{50}$$

2.2.2. Exact vacuum expectation values

The form factors are normalized with their vacuum expectation values (VEVs), so here we determine them. The exact VEV of the bulk field of the scaling Lee–Yang theory is known from conformal perturbation theory and from TBA in the ultraviolet limit [29].

Since the VEV of the bulk field does not depend on its location and the defect fields $\Phi_\pm$ correspond to its limits, we conclude that

$$\langle \Phi \rangle = \langle \Phi_+ \rangle = \langle \Phi_- \rangle = \frac{1}{\pi\lambda(1-h)}\frac{\pi}{4\sqrt{3}}m^2 \simeq 1.23939m^{2h} \tag{51}$$

In order to obtain the expectation values of the chiral fields $\varphi, \bar{\varphi}$, we adopt an argument similar to [12]. The vacuum energy of the system can be generically parametrized as [3]

$$E_0(L) = e_d(b) + LE_{bulk} + E_0^{TBA}(L) \tag{52}$$

where the bulk energy constant is $E_{bulk} = -\frac{1}{4\sqrt{3}}m^2$, the defect energy is given in (29) and $E_0^{TBA}(L)$ is the ground-state energy in the TBA scheme, given in (102) below.

The presence of an integrable defect does not destroy the existence of momentum, merely modifies the momentum eigenvalues, yielding a nonzero value in the ground state. In the same way as for the defect energy, this defect momentum can be conveniently extracted in the ultraviolet limit, if one makes use of the expression

$$P_0^{TBA}(L) = -\frac{m}{2\pi}\int d\theta \sinh\theta \log\left(1 + e^{-\tilde{\epsilon}(\theta)}\right) = P_0(L) - p_d(b) \tag{53}$$

for the exact finite-volume ground state momentum. Here $\tilde{\epsilon}$ satisfies the ground-state TBA equation (see also Section 5)

$$\tilde{\epsilon}(\theta) = mL\cosh\theta - \log T_+\left(\frac{i\pi}{2} - \theta\right) - \varphi(\theta) \star \log\left(1 + e^{-\tilde{\epsilon}(\theta)}\right);$$

$$\varphi(\theta) = -\frac{i}{2\pi}\partial_\theta \log S(\theta) \tag{54}$$

In the $L \to 0$ limit, the solution of (54) develops two plateau regions, which grow as $\sim\log\frac{2}{mL}$, separated by a breather region around the origin. The plateaus end in two kink regions, which do not contribute to the ground state momentum. We therefore focus onto the central region and make use of the pseudo energy

$$\varepsilon_0(\theta) = \lim_{L \to 0} \tilde{\epsilon}(\theta) \tag{55}$$

describing the root distribution in the deep ultraviolet limit. Expanding the expression (54) with $L = 0$ around $\theta \to \pm\infty$ as in [30,3] produces

$$\varepsilon_0(\theta \to \pm\infty) \simeq -A_\pm e^{\mp\theta} + \varepsilon_* \pm \frac{C}{2\pi} I_\pm e^{\mp\theta} \tag{56}$$

where the asymptotic behavior of the kernel and of the source term of (55) define $\varphi(\theta \to \pm\infty) \sim C e^{\mp\theta}$ and $\log T_+(i\frac{\pi}{2} - \theta \to \pm\infty) \sim A_\pm e^{\mp\theta}$. For the model at hand, $C = -2\sqrt{3}$ and $A_\pm = \mp 2i\,(e^{\pm i\pi\frac{b+1}{6}} + e^{\pm i\pi\frac{b-1}{6}})$. Finally, $\varepsilon_* = \log\frac{1+\sqrt{5}}{2}$ is the plateau value of the limit solution for the pseudo energy and we introduce the notation:

$$I_\pm = \int_{-\infty}^{\infty} d\theta\, e^{\pm\theta} \frac{d}{d\theta} \log\big(1 + e^{-\varepsilon_0(\theta)}\big) \tag{57}$$

We define $Y(\theta) = e^{-\varepsilon_0(\theta)}$, which satisfies the

$$Y\left(\theta + i\frac{\pi}{3}\right) Y\left(\theta - i\frac{\pi}{3}\right) = 1 + Y(\theta), \tag{58}$$

functional relation, i.e. the Lee–Yang Y system [3]. This function has period $\frac{5i\pi}{3}$ in the imaginary direction, hence its asymptotic expansion can only contain powers of $e^{\pm\frac{6}{5}\theta}$: cancellation of the terms proportional to $e^{\pm\theta}$ in (56) allows to compute $I_\pm$ exactly. From the expression (53), one then has

$$\lim_{L \to 0} \frac{P_0^{TBA}}{m} = -\frac{A_+ - A_-}{2C} \tag{59}$$

so that the defect momentum is (29).

As a last step, we take the vacuum expectation values of the Hamiltonian and the momentum operator, (86), (87), and differentiate them with respect to the defect parameter b

$$\frac{\partial}{\partial b}\langle H \rangle = i\frac{\pi}{5}\big(\mu\langle\varphi\rangle - \bar{\mu}\langle\bar{\varphi}\rangle\big) \qquad \frac{\partial}{\partial b}\langle P \rangle = i\frac{\pi}{5}\big(\mu\langle\varphi\rangle + \bar{\mu}\langle\bar{\varphi}\rangle\big) \tag{60}$$

By virtue of (33), (29), we obtain the vacuum expectation values of the fields φ and $\bar{\varphi}$,

$$\langle\varphi\rangle = -\frac{5i}{12\mu} e^{-i\frac{\pi b}{6}} \qquad \langle\bar{\varphi}\rangle = \frac{5i}{12\bar{\mu}} e^{i\frac{\pi b}{6}} \tag{61}$$

which we compare with the numerical values in Section 4. Observe that differentiating in Eq. (60) the exact finite volume ground state energy (52) and ground state momentum (53), instead of their asymptotic values (29), we could exactly derive the complete finite size one point function of the defect operators φ and $\bar{\varphi}$.

2.2.3. Spectral expansion of two-point functions

The form factor expansion for correlation functions has proven to be extremely rapidly convergent in the Lee–Yang theory [30], providing a good estimate for the correlation function

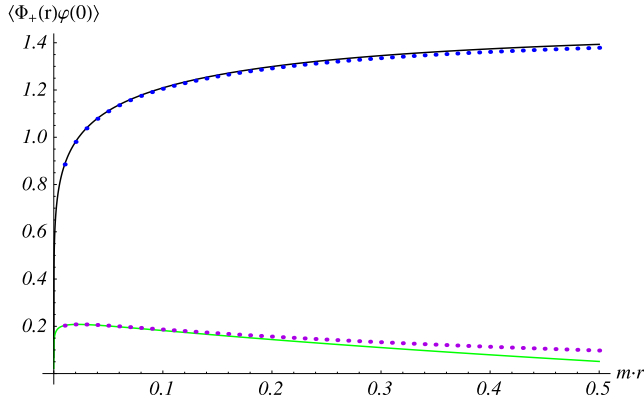$$\big\langle \Phi(x, t)\Phi(0, 0) \big\rangle \tag{62}$$

Fig. 1. $\Phi_+\varphi$ correlation function: blue and purple dots show the real and imaginary part calculated from the form factor expansion up to two particle terms, while black and green curves the first order CFT perturbation results. (For interpretation of the references to color in this figure legend, the reader is referred to the web version of this article.)

up to very small values of the separation between the fields. It is therefore a legitimate check of the form factors expressions, as well as a due comparison of the convergence properties of the spectral expansion in the case of operators living on the defect, to repeat this analysis for the various two-point functions of φ, $\bar{\varphi}$, $\Phi_\pm$.

In the following we analyze the two point functions of local operators $\langle \hat{O}_1(r)\hat{O}_2(0)\rangle$ by inserting a resolution of the identity

$$\langle \hat{O}_1(r)\hat{O}_2(0)\rangle = \sum_{n=0}^{\infty} \langle 0|\hat{O}_1(0)|n\rangle \langle n|\hat{O}_2(0)|0\rangle e^{-E_n r} \tag{63}$$

The various matrix elements are the generic form factors (7), which all can be expressed in terms of the elementary ones. Truncation of the series up to two particle terms gives a good approximation valid even for very small separations, which can be compared to the short distance CFT predictions. In so doing we assume that the local fields in the perturbed theory are in one-to-one correspondence with the operator content of the CFT, apart from additive renormalization constants [30]. The products of fields living on the defect $\hat{O}_1(r)$, $\hat{O}_2(0)$, for small Euclidean time separation, r, can be treated by exploiting their operator product expansion in the short-distance CFT

$$\hat{O}_1(r)\hat{O}_2(0) \sim \sum_j \frac{C_{12}^j \hat{O}_j}{|r|^{h_1+h_2-h_j}} \tag{64}$$

where h_i denote the scaling dimension of the operators and the structure constants C_{12}^j were given in [5]. Knowledge of the exact vacuum expectation values (51), (61), allows one to extract the behavior of the correlation function as $r \to 0$.

We found that the spectral series reproduce the correlation functions to very good accuracy, even for small values of r, by a restricted number of terms only. In the following we focus on the one- and two-particle contributions.

The relevant structure constants are written in terms of the constants $\beta = \sqrt{\frac{2}{1+\sqrt{5}}}$, $\alpha = \sqrt{\frac{\Gamma(1/5)\Gamma(6/5)}{\Gamma(3/5)\Gamma(4/5)}}$ and $\eta = e^{i\frac{\pi}{5}}$. In particular, we show in Fig. 1 the real and imaginary part of the $\Phi_+\varphi$ correlation function, which for short distance is expanded as

$$\langle \Phi_+(r)\varphi(0)\rangle \sim C^{\Phi_+}_{\Phi_+\varphi}\langle \Phi_+\rangle r^{1/5} + C^{\Phi_-}_{\Phi_+\varphi}\langle \Phi_-\rangle r^{1/5} + C^{\bar{\varphi}}_{\Phi_+\varphi}\langle \bar{\varphi}\rangle r^{2/5} \tag{65}$$

with $C^{\Phi_+}_{\Phi_+\varphi} = \frac{\alpha}{2}(\beta+\beta^{-1}+\frac{i}{\sqrt[4]{5}})$, $C^{\Phi_-}_{\Phi_+\varphi} = \frac{\alpha\beta}{2}(1-\frac{i(\beta-\beta^{-1})}{\sqrt[4]{5}})$, $C^{\bar{\varphi}}_{\Phi_+\varphi} = -\frac{\eta}{\beta}$. The short distance CFT expansion is shown with continuous lines, while the form factor expansion with dots. The two point functions of other fields are analyzed in Appendix B.

3. Finite volume form factors: theoretical framework

To verify the predictions made by the defect form factor bootstrap one can use the finite volume form factor formalism developed by Pozsgay and Takacs [23,24]. Based on the description of the finite volume spectrum provided by the Bethe–Yang equations, the formalism gives all finite volume corrections that decay as a power in the inverse volume. The remaining corrections are suppressed exponentially as the volume increases, and at present only a partial description is available for them [27]. In this paper we confine ourselves to the power corrections, as these are sufficient to verify the validity of the defect form factor bootstrap.

3.1. Finite volume energy levels

The finite volume energy levels can be identified with multi-particle states $|\{I_1,\ldots,I_n\}\rangle_L$ containing n particles, labeled by quantum numbers $I_1,\ldots,I_n$ which parametrize the quantization of particle momenta. The quantization conditions satisfied by the particle rapidities θ_k are the Bethe–Yang equations

$$e^{imL\sinh\theta_k}T_-(\theta_k)\prod_{j\neq k}S(\theta_k-\theta_j)=1 \quad k=1,\ldots,n \tag{66}$$

Taking the logarithm, these equations can be rewritten as

$$Q_k(\theta_1,\ldots,\theta_n)_L = 2\pi I_k \quad k=1,\ldots,n \tag{67}$$

where

$$Q_k(\theta_1,\ldots,\theta_n)_L = mL\sinh\theta_k - i\log T_-(\theta_k) - \sum_{j\neq k}i\log S(\theta_k-\theta_j) \tag{68}$$

and the energy is given by

$$E(L) = E_0(L) + \sum_{k=1}^{n}m\cosh\theta_k + O(e^{-\mu L}) \tag{69}$$

where μ is some characteristic scale, and $E_0(L)$ is the ground state (vacuum) energy.

The k-th equation in (67) characterizes the monodromy of the wave functions under moving the k-th particle to the right and around the circle; in doing so, one picks up the phase from crossing the defect, the scattering with the other particles (note the order of the rapidity difference inside S, which corresponds to particle k entering the scattering from the left!). The reason why only $T_-(\theta)$ enters is that it is the phase-shift suffered by a particle of $\theta > 0$ when crossing the defect from the left; on the other hand, if a given particle has $\theta < 0$ its monodromy when crossing from the right to the left would be given by $T_+(-\theta)$; therefore, when crossing from the left to the right the phase-shift is given by

$$T_+(-\theta)^{-1} \tag{70}$$

which is equal to $T_-(\theta)$ by defect unitarity. As a result, Eqs. (67), (68) describe all states in the spectrum by letting the sign of the rapidities free, i.e. by letting I_k to take any integer values. However, due to $S(0) = -1$ the multi-particle wave-functions are non-vanishing only if all the rapidities, and therefore all the quantum numbers, take distinct values.

The density of states in finite volume can be obtained from the Jacobi determinant of the mapping from rapidity space to the space of the quantum numbers:

$$\rho_n(\theta_1, \ldots, \theta_n)_L = \det\left\{ \frac{\partial Q_k(\theta_1, \ldots, \theta_n)_L}{\partial \theta_j} \right\}_{k,j=1,\ldots,n} \tag{71}$$

3.2. Non-diagonal matrix elements

Using the arguments in the work [23], the finite volume matrix elements of a defect operator can be obtained as

$$\langle \{J_1, \ldots, J_n\} | \mathcal{O}(t=0) | \{I_1, \ldots, I_k\} \rangle_L$$
$$= \pm \frac{F^{\mathcal{O}}(\tilde{\theta}'_n + i\pi, \ldots, \tilde{\theta}'_1 + i\pi, \tilde{\theta}_1, \ldots, \tilde{\theta}_k)}{\sqrt{\rho_n(\tilde{\theta}'_1, \ldots, \tilde{\theta}'_n)_L \rho_k(\tilde{\theta}_1, \ldots, \tilde{\theta}_k)_L}} \Phi(\tilde{\theta}'_1, \ldots, \tilde{\theta}'_n)^* \Phi(\tilde{\theta}_1, \ldots, \tilde{\theta}_k) + O(e^{-\mu L}) \tag{72}$$

where $F^{\mathcal{O}}$ is the infinite volume form factor, $\tilde{\theta}_1, \ldots, \tilde{\theta}_k$ and $\tilde{\theta}'_1, \ldots, \tilde{\theta}'_n$ are the solutions to the Bethe–Yang equations (67), (68) with quantum numbers $I_1, \ldots, I_k$ and $J_1, \ldots, J_n$, respectively, and the Φ are phase factors ensuring that the finite volume scattering state is symmetric in its arguments and is invariant under crossing any particle of the defect. Clearly in finite volume the particles are not ordered and are on the left and on the right of the defect in the same time. The correct phase factor with this properties have the form

$$\Phi(\theta_1, \ldots, \theta_n) = \pm \left(\prod_{\substack{j,l=1 \\ j<l}}^{n} S(\theta_j - \theta_l) \prod_{j=1}^{n} T_-(\theta_j) \right)^{-\frac{1}{2}} \tag{73}$$

We remark that the phases Φ have no physical significance as they cancel in any correlation function computed in the theory, whether in finite or infinite volume; it is only necessary to keep track of them when analytically continuing (72) to complex values of the rapidities, as in [21,27]. Finally, the $\pm$ sign results from the ambiguity in choosing the branch of the square root functions; the same ambiguity is present in TCSA as the eigenvectors still have a residual sign ambiguity even after imposing a suitable reality condition.

In the case of the Lee–Yang model we have a physical normalization of the TCSA eigenvectors. We chose the normalization of the UV primary defect creating fields as

$$C^{\mathbb{I}}_{dd} = C^{\mathbb{I}}_{\bar{d}\bar{d}} = 1; \qquad C^{\mathbb{I}}_{DD} = -1, \tag{74}$$

the same way as in [5]. The ground state of the perturbed CFT flows to the lowest energy state in the UV limit which is the field D with negative squared norm. This is therefore natural to chose the ground state TCSA vectors at any volume to be purely imaginary.

The second and the third lowest energy states in the TCSA (which correspond to the slowest left- and right-moving one particle states in the scattering theory point of view) never cross any

other lines at any volume, therefore, they flow to the second and the third lowest energy states in the conformal theory, namely $|d\rangle$ and $|\bar{d}\rangle$. Consequently we normalized the corresponding TCSA vectors to be real.

In the UV limit the states of the Verma modules built over the highest weight states d and $\bar{d}$ are related by parity transformation while the Verma module of D is parity symmetric. In case of a parity symmetric defect the only parity symmetric states in the scattering theory are the even particle states composed by particles with opposite rapidities, so these states flow to some parity symmetric state in the D-module. These arguments suggest us that the even particle TCSA states flow to the D-module while the odd particle TCSA states to either to the d-module or to the $\bar{d}$-module in the conformal limit. For this reason we normalized the even particle TCSA states to be purely imaginary while the odd particle states to be real. This assumption is tested *a posteriori*, measuring the phases (or equivalently both the real and imaginary part) of the form factors from the TCSA and comparing them to the theoretically computed finite volume form factors allow us a non-trivial check, and we found a perfect agreement for all the studied states.

For bulk operators, the extension of (72) is simple. As noted in [4], the presence of an integrable defect only breaks translational invariance by having a defect momentum p_D (in addition to a defect energy E_D). The total momentum, which includes the defect momentum as well, is conserved; therefore the space–time dependence of a bulk operator can be computed by multiplying (72) by the phase factor

$$e^{-it\Delta E + ix\Delta P} \tag{75}$$

where

$$\Delta E = \sum_{i=1}^{k} m\cosh\tilde{\theta}_i - \sum_{j=1}^{n} m\cosh\tilde{\theta}'_j$$

$$\Delta P = \sum_{i=1}^{k} m\sinh\tilde{\theta}_i - \sum_{j=1}^{n} m\sinh\tilde{\theta}'_j \tag{76}$$

3.3. Diagonal matrix elements

Formula (72) is valid if there are no disconnected terms in the matrix element. Disconnected terms arise when there is at least one rapidity value among the $\tilde{\theta}_1, \ldots, \tilde{\theta}_m$ which coincides with a value occurring in $\tilde{\theta}'_1, \ldots, \tilde{\theta}'_n$. Following two energy levels as the volume L varies, this can occur at particular isolated values of L, but these cases are not interesting as the matrix element can be evaluated by taking the limit of (72) in the volume. Therefore the only interesting cases are when disconnected terms are present for a continuous range of the volume L. Due to the presence of interactions (the S terms) in (67), (68) this can only occur in very specific situations; the only generic class is when the matrix element is diagonal, i.e. the two states are eventually identical, in which case disconnected terms are present for all values of L.

In this case, we can proceed by analogy to the bulk and boundary cases. For diagonal matrix elements

$$\langle\{I_1, \ldots, I_n\}|\mathcal{O}|\{I_1, \ldots, I_n\}\rangle_L \tag{77}$$

Eq. (72) shows that the relevant form factor expression is

$$F^{\mathcal{O}}(\theta_n + i\pi, \ldots, \theta_1 + i\pi, \theta_1, \ldots, \theta_n) \tag{78}$$

Due to the existence of kinematical poles this must be regularized; however the end result depends on the direction of the limit. The terms that are relevant in the limit can be written in the following general form:

$$F^{\mathcal{O}}(\theta_n + i\pi + \epsilon_n, \ldots, \theta_1 + i\pi + \epsilon_1, \theta_1, \ldots, \theta_n)$$
$$= \prod_{i=1}^{n} \frac{1}{\epsilon_i} \cdot \sum_{i_1=1}^{n} \cdots \sum_{i_n=1}^{n} \mathcal{A}_{i_1 \ldots i_n}(\theta_1, \ldots, \theta_n) \epsilon_{i_1} \epsilon_{i_2} \ldots \epsilon_{i_n} + \cdots \tag{79}$$

where $\mathcal{A}_{i_1 \ldots i_n}^{a_1 \ldots a_n}$ is a completely symmetric tensor of rank n in the indices $i_1, \ldots, i_n$, and the ellipsis denote terms that vanish when taking $\epsilon_i \to 0$ simultaneously.

The connected matrix element can be identified as the ϵ_i independent part of Eq. (79), i.e. the part which does not diverge whenever any of the ϵ_i is taken to zero:

$$F_{conn}^{\mathcal{O}}(\theta_1, \theta_2, \ldots, \theta_n) = n! \mathcal{A}_{1 \ldots n}(\theta_1, \ldots, \theta_n) \tag{80}$$

where the appearance of the factor $n!$ is simply due to the permutations of the ϵ_i.

Following [24,16], we are lead to the following expression

$$\big\langle \{I_1 \ldots I_n\} \big| \mathcal{O} \big| \{I_1 \ldots I_n\} \big\rangle_L$$
$$= \frac{1}{\rho_n(\tilde{\theta}_1, \ldots, \tilde{\theta}_n)_L} \sum_{A \subset \{1,2,\ldots n\}} F_{conn}^{\mathcal{O}}\big(\{\tilde{\theta}_k\}_{k \in A}\big) \tilde{\rho}_n(\tilde{\theta}_1, \ldots, \tilde{\theta}_n | A)_L + O\big(e^{-\mu L}\big) \tag{81}$$

where the summation runs over all subsets A of $\{1, 2, \ldots, n\}$, and $\{\tilde{\theta}_1, \ldots, \tilde{\theta}_n\}$ are the Bethe–Yang rapidities corresponding to the set of quantum numbers $\{I_1, \ldots, I_n\}$. For any such subset, we define the appropriate sub-determinant

$$\tilde{\rho}_n(\tilde{\theta}_1, \ldots, \tilde{\theta}_n | A) = \det \mathcal{J}_A(\tilde{\theta}_1, \ldots, \tilde{\theta}_n) \tag{82}$$

of the $n \times n$ Bethe–Yang Jacobi matrix

$$\mathcal{J}(\tilde{\theta}_1, \ldots, \tilde{\theta}_n)_{kl} = \frac{\partial Q_k(\theta_1, \ldots, \theta_n)_L}{\partial \theta_l} \tag{83}$$

where $\mathcal{J}_A$ is obtained by deleting the rows and columns corresponding to the subset of indices A. The determinant of the empty sub-matrix (i.e. when $A = \{1, 2, \ldots n\}$) is defined to equal to 1 by convention. Note also that diagonal matrix elements have no space–time dependence at all, therefore (81) is true both for operators located on the defect and in the bulk.

We note for bulk theories on a spatial circle without defects, that there exists another class of matrix elements with disconnected contributions when there is a particle of exactly zero momentum in both states. However, due to the presence of the defect this class is absent here. For example, from (66) it follows that the existence of a state with a single stationary particle would require

$$T_-(\theta = 0) = 1 \tag{84}$$

but this is not satisfied for any finite value of the defect parameter b. The only class of matrix elements that has disconnected pieces at more than isolated values of L is the diagonal one treated above.

4. Numerical comparison

A valuable tool for investigating statistical field theories in the vicinity of the critical point was devised in [28] and successfully tested on the scaling Lee–Yang theory. Being based on the knowledge of the Hilbert space at the conformal point, where the spectrum is discrete, and on the truncation of the constituting Verma modules at a certain level m, it has been dubbed truncated conformal space approach (TCSA).

In the present case, the Hilbert space is spanned by the defect-creating operators, whose corresponding hw. states are denoted by $|D\rangle, |d\rangle, |\bar{d}\rangle$ in [5], with conformal dimensions $(h, \bar{h}) = (-\frac{1}{5}, -\frac{1}{5}), (-\frac{1}{5}, 0), (0, -\frac{1}{5})$.

In order to evaluate matrix elements of the Hamiltonian, the theory is mapped on the plane by the transformation

$$z = e^{-i\frac{2\pi}{L}\zeta}, \qquad \bar{z} = e^{i\frac{2\pi}{L}\bar{\zeta}} \tag{85}$$

where $\zeta = x + iy$ and $\bar{\zeta} = x - iy$ are the Euclidean coordinates on the cylinder. Operators will appear as finite-size matrices on the states $|j\rangle$ of the conformal Hilbert space on the plane and the Hamiltonian and momentum operators read

$$\frac{H}{m} = \frac{2\pi}{mL}\left(L_0 + \bar{L}_0 + \frac{11}{30} + \xi\left(\frac{L}{2\pi\kappa}\right)^{1+\frac{1}{5}}\left(a(G^{-1}\hat{\varphi})_{jk} + \bar{a}(G^{-1}\hat{\bar{\varphi}})_{jk}\right)\right.$$
$$\left. + \left(\frac{L}{2\pi\kappa}\right)^{2+\frac{2}{5}}(G^{-1}\Phi)_{jk}\right) \tag{86}$$

$$\frac{P}{m} = \frac{2\pi}{mL}\left(L_0 - \bar{L}_0 + \xi\left(\frac{L}{2\pi\kappa}\right)^{1+\frac{1}{5}}\left(a(G^{-1}\hat{\varphi})_{jk} - \bar{a}(G^{-1}\hat{\bar{\varphi}})_{jk}\right)\right) \tag{87}$$

where $G_{jk} = \langle j|k\rangle, \hat{\varphi}_{jk} = \langle j|\varphi(1)|k\rangle, \hat{\bar{\varphi}}_{jk} = \langle j|\bar{\varphi}(1)|k\rangle, \hat{\Phi}_{jk} = \langle j|\Phi(1,1)|k\rangle P_{jk}$ and the matrix

$$P_{jk} = \begin{cases} -2\pi & \text{if } h_k - \bar{h}_k - h_j + \bar{h}_j = 0 \\ -2e^{-i\pi(h_k - \bar{h}_k - h_j + \bar{h}_j)}\frac{\sin\pi(h_k - \bar{h}_k - h_j + \bar{h}_j)}{(h_k - \bar{h}_k - h_j + \bar{h}_j)} & \text{otherwise} \end{cases} \tag{88}$$

is obtained by performing the integration on the spatial coordinate of the bulk perturbing field. Also, there appear the parameters $\kappa = \frac{2^{19/12}\sqrt{\pi}(\Gamma(\frac{3}{5})\Gamma(\frac{4}{5}))^{5/12}}{5^{5/16}\Gamma(\frac{2}{3})\Gamma(\frac{5}{6})}, \xi = \sqrt[4]{\frac{5}{8} + \frac{3\sqrt{5}}{8}}, a = e^{-i\frac{\pi}{5}(b-2)}$ and $\bar{a} = e^{i\frac{\pi}{5}(b-2)}$.

Diagonalization of the truncated Hamiltonian yields the energy levels, which can be compared with the corresponding quantities obtained from Bethe–Yang equation (66), finding excellent agreement in all intermediate regimes [5].

Truncation of the Hilbert space introduces an error in the computation of energy levels and matrix elements. However, at least for an operator with weight $h, \bar{h} < \frac{1}{2}$, such an error is expected to be smaller and smaller as the truncation level is increased. We found that, due to the rapid growth of the Hilbert space and the consequent processor memory usage, it was impossible for us to go beyond truncation level $n = 18$, where the effects due to the finiteness of the space are still noticeable. This forced us to improve the precision by renormalization group (RG) methods.

A renormalization group for the truncation level dependence was introduced in [13,15,14] and extended to VEVs in [26]. Here we briefly repeat the basic steps of the derivation in [26]

for matrix elements with the perturbed action (26), and refer to the original derivation for more extensive explanation of the procedure.

The matrix element of a given local operator $\mathcal{O}$, represented on a finite-dimensional space, will be denoted by

$$O_{ab}(n) = \langle a | P_n \mathcal{O}(0,0) P_n e^{-\lambda \int d^2 r\, V(\vec{r}) - \eta \int dt\, W(t)} P_n | b \rangle \tag{89}$$

where the last factor in the expectation value represents a combined bulk and defect perturbation, as in (26), the operator P_n is a projector onto the states up to level n, and the operator products are assumed to be time ordered.

The idea is to study the difference $O_{ab}(n+1) - O_{ab}(n)$ by perturbation theory using that the couplings λ, η are relevant, and so when the descendant states at the cutoff level n have energy much higher than the mass gap $\frac{4\pi n}{L} \gg m$ their effect can be taken into account perturbatively. The bulk perturbation has already been analyzed in the original literature and the method can be straightforwardly extended to a combined bulk and defect perturbation; we concentrate here on the defect part, and only present the main differences with respect to the original derivation in [26]. It is possible to consider separately the two components of the perturbation because the (projected) parts of the evolution operators associated with the two perturbations commute to first order in λ, η. As a first step, we write the matrix element in the form

$$Q_{ab}(n) = \langle a | U_+^{(n)}(\eta) P_n O(0) P_n U_-^{(n)}(\eta) | b \rangle \tag{90}$$

where $U_\pm^{(n)}$ are past and future evolution operators at a given cutoff. We evaluate the difference

$$
\begin{aligned}
& Q_{ab}(n+1) - Q_{ab}(n) \\
&= -2\eta \left(\frac{L}{2\pi} \right)^{1 - h_W - \bar{h}_W} \\
&\quad \times \int_0^1 d\rho\, \rho^{-1 + h_W + \bar{h}_W} \langle a | U_+^{(n)}(\eta) O(1) (P_{n+1} - P_n) W(\rho) U_-^{(n)}(\eta) | b \rangle + O(\eta^2)
\end{aligned}
\tag{91}
$$

where we applied the exponential map (85), with $z = \rho e^{i\gamma}$ and put the defect at the radius $\gamma = 0$. We then use the operator product expansion

$$O(0) W(z) = \sum_A \frac{C_{OW}^A A(0)}{|1 - \rho|^{h_O + h_W - h_A + \bar{h}_O + \bar{h}_W - \bar{h}_A}} \tag{92}$$

where the summation runs over the scaling fields of the Hilbert space at the conformal point, while the C_{OW}^A are the associated structure constants. In the above expression, the projector on the n-th level singles out the corresponding descendants in the sum, and after further manipulations in the limit $n \gg 1$, one obtains

$$\frac{d}{dn} Q_{ab}(n) \propto \sum_A K_A n^{h_O + h_W - h_A + \bar{h}_O + \bar{h}_W - \bar{h}_A - 2} \tag{93}$$

which implies that truncation errors, in the case of a defect perturbation, decay as

$$Q_{ab}(n) = Q_{ab}(\infty) + \sum_A \tilde{K}_A n^{h_O + h_W - h_A + \bar{h}_O + \bar{h}_W - \bar{h}_A - 1} \tag{94}$$

Conversely, in the case in which the action contains a bulk perturbation only, it was found that

$$Q(n) = Q(\infty) + \sum_A \tilde{K}_A n^{h_O + h_W - h_A + \bar{h}_O + \bar{h}_W - \bar{h}_A - 2} \tag{95}$$

which shows why truncation effects from the defect perturbation are generically more relevant than those resulting from the bulk perturbation.

For practical reasons, since the sub-leading terms which are not taken into account in the formula above are $O(1/n)$, one retains in the sum only the most relevant defect fields, which correspond to the leading terms for large n.

Understanding the behavior of the matrix elements allows to extrapolate their value when the cutoff in the state number tends to infinity and allows comparison with the quantities computed in Section 3. Explicit examples can be obtained by using the OPE given in [5]: in the case of φ and $\bar{\varphi}$, the slowest correction arises from the presence of the $\Phi_\pm$ channel in the OPE of φ and $\bar{\varphi}$ and gives a power of n^{-1}; conversely, from the fact that the structure constants $C_{\Phi_\pm\varphi}^{\bar{\varphi}}$, $C_{\Phi_\pm\bar{\varphi}}^{\varphi}$ are different from zero, one obtains that the cut-off dependence vanishes as $n^{-6/5}$ for $\Phi_\pm$.

4.1. Vacuum expectation values

We would like to compare the expectation values of the fields $\Phi_\pm$, φ, $\bar{\varphi}$ derived in Section 2.2.2, to the data extracted from TCSA. Throughout this section, we work at a fixed value of $b = -3 + 0.5i$. As explained in [5], such a value ensures a real spectrum, thereby facilitating the comparison between the energy and momentum data computed from the Bethe–Yang equations and from TCSA. We chose a value of the defect parameter with a small imaginary part in order to avoid the occurrence of degenerate subspaces (corresponding, in the infrared, to particles traveling with opposite rapidity). In the form factor comparison we are interested not only in the eigenvalues but also in the eigenvectors of the TCSA energy and momentum. As energy levels might be degenerate for specific volumes the identification and systematic tracking of states can be problematic. To avoid this we combine the self-adjoint H and P into $H + iP$, which has nondegenerate complex spectrum, and by following its eigenstates we could identify 127 states (up to four-particle ones) from TCSA.

In the following we present the real and imaginary parts of measured, extrapolated and theoretically calculated form factors. All of them have the same consistent legend: green color shows the real part of measured form factors at cut level 12, 14, 16, 18 ($\bullet$, $\blacksquare$, $\blacklozenge$, $\blacktriangle$); red squares show the real part of extrapolated data with confidence intervals; and black line shows the real part of theoretical values. The imaginary parts have the same structure, with colors purple, blue and orange, respectively.

Concerning the confidence intervals we used Mathematica 9 to fit the leading cut dependence via (95). We found that the real and imaginary parts are basically not correlated thus we fit them separately. On all the figures the confidence level is 95%. The theoretical data can be outside the confidence interval for two reasons. For small volumes the TCSA data are reliable but the exponentially suppressed vacuum polarization effects of the form factor are no longer negligible. For large volume the finite volume form factors are reliable but the sub-leading TCSA cut dependence becomes relevant.

First, we present an example of how the extrapolation procedure works in the case of the defect field φ. In Fig. 2, we show the TCSA data and the extrapolated value together with the theoretical value for cylinder sizes between 0.2 and 20.

We report below the numerical comparison between the exact expectation values of the operators living on the defect and the ones extrapolated at a large enough volume $mL = 15$, such that the exponential finite-size corrections can be safely neglected (Table 2).
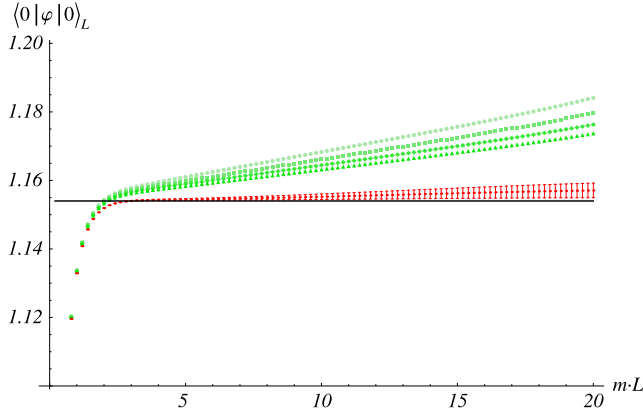
Fig. 2. Comparison between the TCSA points at different cuts, the extrapolated values and the theoretical vacuum expectation value of φ.

Table 2
Numerical comparison of the TCSA extrapolated and the theoretical values of the vacuum expectation values of different operators at volume $mL = 15$.

	φ	$\bar{\varphi}$	Φ_+
TCSA extrapolated VEV	1.2795	1.1529	1.2368
Theoretical VEV	1.2814	1.154	1.2394

4.2. One particle form factors

We now turn to one-particle form factors, which, in the presence of a defect, already carry a nontrivial dependence on the rapidity of the particle due to the transmission factors from Section 2.1 above.

We can collect extrapolated data from states labeled by different quantization numbers and from different volumes (from 4 to 20). The particle rapidity in a given state is determined from the BY equation (66). From this, it is known how to relate the finite volume matrix elements and the infinite volume form factors, through (72).

We now examine the one-particle form factors of the fields φ and $\bar{\varphi}$. Following the procedure outlined above, we obtain confirmation of the expected θ-dependence.

Tho similar analysis for the one particle form factors of the operators $\Phi_\pm$ can be found in Appendix B.

4.3. Multiparticle form factors

Analogously to the one particle form factors above we can check the two or more particles form factors. However, they will generally depend on more than one rapidities separately. For this reason it is easier to analyze the volume dependence of a form factor for a given state, identified by the quantization numbers of its rapidities in the Bethe–Yang equation (66). Such lines are identified from the corresponding energy and momentum levels. Here below, we present some examples of different states (Figs. 3–5). A more exhaustive list of data can be found in Appendix B.
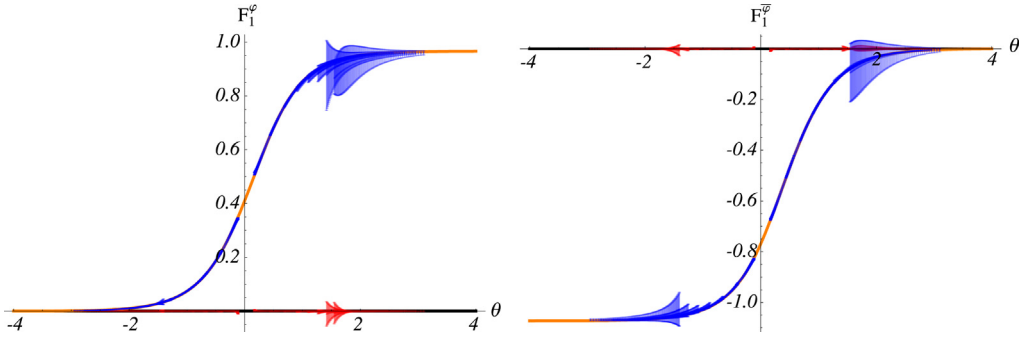
Fig. 3. Comparison between the extrapolated TCSA data (dots with confidence bars) and the theoretical prediction (solid line) for the one-particle form factor of the operators φ and $\bar{\varphi}$.
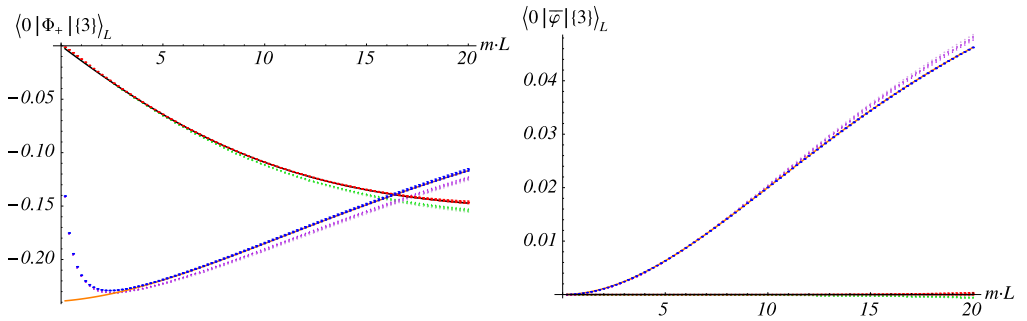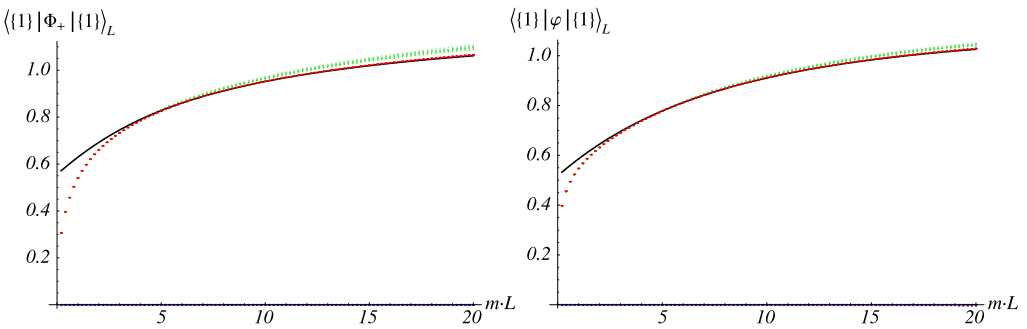

Fig. 4. Left: one-particle form factor of the operator Φ_+ on the state labeled by quantum number $n_1 = 3$. Right: one-particle form factor of the operator $\bar{\varphi}$ on the state $n_1 = 3$. The solid lines are computed from formula (72), while the dots with confidence bars are obtained by extrapolated TCSA data. (The consistent legend is described in the beginning of Section 4.1.)

Fig. 5. Left: one-particle diagonal form factor of the operator Φ_+ on the state labeled by quantum number $n_1 = 1$. Right: one-particle diagonal form factor of the operator φ on the state $n_1 = 1$. The solid lines are computed from formula (81), while the dots with confidence bars are obtained by extrapolated TCSA data. (The consistent legend is described in the beginning of Section 4.1.)

We remark that the extrapolation fails for very large values of the dimensionless volume mL. The reason is that for relevant perturbing fields the dimensionless couplings in the Hamiltonian

depends on a positive power of the coupling, and therefore perturbation theory is only applicable when the condition

$$\frac{4\pi n}{mL} \gg 1 \tag{96}$$

is satisfied [26]; if this is not the case, it is necessary to evaluate the cutoff dependence to higher orders in perturbation theory, which is a very complicated task and out of the scope of the present work. These extra terms appear during the extrapolation procedure as systematic errors, and this is why the confidence intervals calculated during data fittings do not always contain the theoretical data (mainly for larger volumes). However these confidence intervals were kept, because usually they correctly reflect the reliability of TCSA method.

4.4. Diagonal form factors

To calculate the diagonal form factors in finite volume we need the connected form factors defined in Eq. (80). We can make use of the identities (38) and (41) to simplify these expressions. For operators $\Phi_\pm$ we get

$$F_{2n,c}^{\Phi_\pm}(\theta_1, \ldots, \theta_n) = \langle \Phi \rangle \left(\frac{\sqrt[4]{3}i}{\sqrt{2}v(0)} \right)^{2n} f(i\pi)^n \frac{Q_n^{\Phi_\pm}(\theta_1, \ldots, \theta_n)}{\prod_{j<k}^n (\sinh^2(\theta_j - \theta_k) + \sin^2(\frac{\pi}{3}))} \tag{97}$$

with $Q_n^{\Phi_\pm}$ given in Eq. (46).

Here we show the one particle diagonal matrix elements. The multiparticle matrix elements up to four particle number can be found in Appendix B.

5. Expectation values in finite volume/temperature

In this section we derive the exact finite volume vacuum expectation value of our fields. We follow the derivation in [25] and indicate the slight modifications only. We start with an operator, $\mathcal{O}$, localized in the bulk at $x = -1$ and $y = 0$. The defect is localized at $x = 0$ and the size of our system is L. As usual we do the calculation on the torus by exchanging the role of space and time:

$$_L\langle 0|\mathcal{O}(-1, 0)|0\rangle_L = \lim_{R \to \infty} \frac{\text{Tr}(\mathcal{O}(0, -1)e^{-H(R)L}D)}{\text{Tr}(e^{-H(R)L}D)} \tag{98}$$

In the mirror (exchanged) theory the defect acts like an operator, which we denote by D. As the location of the defect operator is irrelevant we can follow the derivation of the defect TBA equation [3] to redefine the Hamiltonian to be

$$\tilde{H}(R) = H(R) - \frac{1}{L}\log D. \tag{99}$$

This will have no other effect then to change the dispersion relation as

$$m\cosh\theta \to m\cosh\theta - \frac{1}{L}\log T_+\left(\frac{i\pi}{2} - \theta\right) \tag{100}$$

With these changes the TBA equation takes the form

$$\tilde{\epsilon}(\theta) = mL\cosh\theta - \log T_+\left(\frac{i\pi}{2} - \theta\right) - \int_{-\infty}^{\infty} \frac{d\theta'}{2I\pi}\varphi(\theta - \theta')\log(1 + e^{-\tilde{\epsilon}(\theta')}) \tag{101}$$
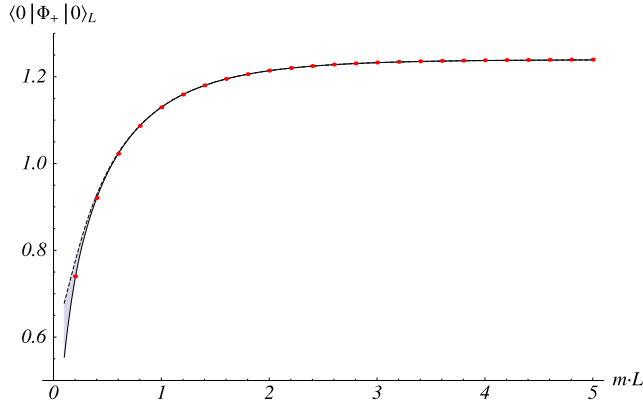
Fig. 6. Comparison of the TCSA data (red dots) to the prediction from the series (103) up to 3 terms (black curve) and up to 2 terms (black dashed curve) for the finite-volume vacuum expectation value of the fields $\Phi_{\pm}$. (For interpretation of the references to color in this figure legend, the reader is referred to the web version of this article.)

giving the ground state energy as

$$E_0^{TBA}(L) = -m \int\limits_{-\infty}^{\infty} \frac{d\theta}{2\pi} \cosh(\theta) \log\big(1 + e^{-\tilde{\epsilon}(\theta)}\big) \tag{102}$$

The only deference compared to the periodic situation is that the pseudo energy has changed. Thus the derivation of [25] will lead to the result

$$_L\langle 0|\mathcal{O}|0\rangle_L = \sum_{n=0}^{\infty} \frac{1}{n!} \prod_{j=1}^{n} \int \frac{d\theta_j}{2\pi} \frac{1}{1 + e^{\tilde{\epsilon}(\theta_j)}} F_{2n}^C(\theta_1, \ldots, \theta_n) \tag{103}$$

for the exact finite volume vacuum expectation value of any bulk operator. Clearly this results holds for the two limits $\Phi_{\pm}$ of the bulk field. The calculation of the exact finite volume vacuum expectation values of the defect fields φ and $\bar{\varphi}$ follows from the exact ground state energy and momentum as we explained at the end of Section 2.2.2.

As far as the fields $\Phi_{\pm}$ are concerned, the knowledge of the form factors of the trace of the bulk stress tensor [30] is sufficient to exploit the connected multi-particle form factors.

The numerical comparison goes in two steps: first, we solve Eq. (101) iteratively for the pseudo energy, starting from a trial solution containing only the hyperbolic term in large volume and decreasing the volume gradually. Then, we compute the series (103) with the form factors given above. In Fig. 6, we show a comparison between the extrapolated one-point function of the field $\Phi_{\pm}$ and the corresponding defect LeClair–Mussardo series, up to three-particle contributions. Note that the outcome of the procedure is different from the bulk case.

The numerical values of these points, for more precise comparison, are reported in Fig. 7.

6. Conclusions

We developed the theory of finite volume form factors in the presence of integrable defects. Our framework is valid for large volumes and takes into account all polynomial finite size corrections but neglects the exponentially small effects. We expressed these finite volume form factors in terms of the infinite volume form factors and the finite volume density of states, which depends on the scattering and transmission matrices.

mL	DLM	DTCSA
1	1.12971	1.12944
2	1.21394	1.21368
3	1.23245	1.23216
4	1.23733	1.23705
5	1.23875	1.23851
6	1.23919	1.23901
7	1.23933	1.23925
8	1.23937	1.23942
9	1.23939	1.23957
10	1.23939	1.23972

Fig. 7. Numerical values for Fig. 6.

We tested these ideas in the Lee–Yang model against the data of the truncated conformal space approach. Within this framework, we numerically diagonalized the Hamiltonian of the finite volume system on a truncated Hilbert space and evaluated the matrix elements of local operators. We performed a systematic comparison: first we compared the vacuum expectation values of all local fields. In so doing we derived exact explicit expressions for the vacuum expectation values of all of the defects fields. We then determined all form factors of the defects fields. We used these results to calculate the two point functions of defect fields, which we compared to the short distance expansion, which contains information on the conformal structure constants and the vacuum expectation values. We also compared the finite volume form factors against the TCSA data. Finally, we derived an explicit expression for the exact finite volume vacuum expectation value of any defect operator in terms of the multi-particle form factors and the defect thermodynamic Bethe Ansatz pseudo energy, which we also checked numerically. In all of these comparisons we used a renormalization group-improved version of TCSA, which we adapted to the present case, and found excellent agreement.

Our methods developed for the Lee–Yang model have a much wider application and can be directly generalized for any diagonal scattering theories. Especially, the parametrization of the defect form factors in terms of the bulk form factors and extra polynomials should be applied to other models. The generalization of our approach for non-diagonal theories is a non-trivial and rather interesting problem. As the transmission matrix bootstrap program was completed for many purely transmitting defect theories [7,9,8], it would be nice to formulate and solve their form factor bootstrap program, too.

Here we analyzed only the polynomial corrections in the inverse of the volume for the finite volume form factors. It is a challenging problem to calculate systematically the exponentially small finite size correction.

Acknowledgements

Appendix A. Exact form factor solutions

In this appendix we present all form factors of primary operators. The two limits of the bulk fields $\Phi_\pm$ are the simplest as they can be expressed in terms of the bulk form factors. For this reason we recall the bulk form factors first.

A.1. Bulk form factors

Bulk form factors of the operator Φ are parametrized as

$$B_n(\theta_1, \ldots, \theta_n) = \langle \Phi \rangle H_n \prod_{i<j} \frac{f(\theta_i - \theta_j)}{x_i + x_j} Q_n^{bulk}(x_1, \ldots, x_n) \tag{104}$$

In the Lee–Yang model Φ is the perturbing operator itself, thus it is proportional to the trace of the energy–momentum tensor. As a consequence the form factor must have the form

$$Q_1^{bulk}(x_1) = 1 \tag{105}$$

$$Q_2^{bulk}(x_1, x_2) = \sigma_1^{(2)}(x_1, x_2) \tag{106}$$

$$Q_n^{bulk}(x_1, \ldots, x_n) = \sigma_1^{(n)}(x_1, \ldots, x_n)\sigma_{n-1}^{(n)}(x_1, \ldots, x_n) P_n(x_1, \ldots, x_n) \quad \text{if } n \geqslant 3 \tag{107}$$

where the P_n polynomials satisfy the following recurrence relations

$$P_{n+2}(x, -x, x_1, \ldots, x_n) = \frac{(\prod_{i=1}^n (x + \omega x_i)(x - \bar{\omega} x_i) - \prod_{i=1}^n (x - \omega x_i)(x + \bar{\omega} x_i))}{2x(\omega - \bar{\omega})}$$

$$\times (-1)^{n+1} P_n(x_1, \ldots, x_n) \tag{108}$$

$$P_{n+1}(\omega x, \bar{\omega} x, x_1, \ldots, x_n) = \prod_{i=1}^{n-1} (x + x_i) P_n(x, x_1, \ldots, x_n) \tag{109}$$

The solution of this recursion can be written in terms of a determinant:

$$P_n(x_1, \ldots, x_n) = \det \Sigma^{(n)}, \qquad \Sigma_{ij}^{(n)}(x_1, \ldots, x_n) = \sigma_{3i-2j+1}^{(n)}(x_1, \ldots, x_n) \tag{110}$$

A.2. Form factors of $\Phi_{\pm}$

Based on our previous discussion the form factor of Φ_- is the bulk form factor:

$$F_n^{\Phi_-}(\theta_1, \ldots, \theta_n) = B_n(\theta_1, \ldots, \theta_n) \tag{111}$$

while the form factor is Φ_+ is of the form

$$F_n^{\Phi_+}(\theta_1, \ldots, \theta_n) = \prod_n T_-(\theta_i) B_n(\theta_1, \ldots, \theta_n) \tag{112}$$

Comparing the parametrization of the bulk and defect form factors we can conclude that

$$Q_n^{\Phi_{\pm}}(x_1, \ldots, x_n)$$
$$= \prod_{i=1}^n (\nu x_i + \bar{\nu} x_i^{-1} \mp \sqrt{3}) Q_n^{bulk}(x_1, \ldots, x_n)$$
$$\times \prod_{i=1}^n (\nu x_i + \bar{\nu} x_n^{-1} \mp \sqrt{3})\sigma_1^{(n)}(x_1, \ldots, x_n)\sigma_{n-1}^{(n)}(x_1, \ldots, x_n) P_n(x_1, \ldots, x_n) \tag{113}$$

A.3. Form factors of $\bar{\varphi}$ and φ

Let's focus on the form factor solutions for a generic defect field. Calculating explicitly the first few Q polynomials we found for φ:

$$Q_1^{\varphi} = \nu\sigma_1$$
$$Q_2^{\varphi} = \sigma_1 + \nu^2\sigma_1\sigma_2$$
$$Q_3^{\varphi} = \bar{\nu}\sigma_1^2 + \nu\sigma_1^2\sigma_2 + \nu^3\sigma_1\sigma_2\sigma_3$$
$$Q_4^{\varphi} = \bar{\nu}^2\sigma_1^2\sigma_2 + \sigma_1^2\sigma_2^2 + \nu^2\sigma_1\sigma_2^2\sigma_3 + \nu^4\sigma_1\sigma_2\sigma_3\sigma_4$$
$$Q_5^{\varphi} = \bar{\nu}^3\big(\sigma_1^2\sigma_2\sigma_3 - \sigma_1^2\sigma_5\big) + \bar{\nu}\big(\sigma_1^2\sigma_2^2\sigma_3 - \sigma_1^2\sigma_2\sigma_5\big) + \nu\big(\sigma_1\sigma_5^2 + \sigma_1\sigma_2^2\sigma_3^2 - 2\sigma_1\sigma_2\sigma_3\sigma_5\big)$$
$$+ \nu^3\big(\sigma_1\sigma_2\sigma_3^2\sigma_4 - \sigma_1\sigma_3\sigma_4\sigma_5\big) + \nu^5\big(\sigma_1\sigma_2\sigma_3\sigma_4\sigma_5 - \sigma_1\sigma_4\sigma_5^2\big) \tag{114}$$

where at each level $n = 1, \ldots, 5$ we abbreviated $\sigma_k^{(n)}$ by σ_k.

These explicit solutions suggest to parametrize the general form factors as

$$Q_n(n) = R\big(\sigma_1^{(n)}, \bar{\sigma}_1^{(n)}\big)\sigma_n^{(n)} P_n^{(n)} S_n^{(n)} \tag{115}$$

for $n \geqslant 3$, where R is some polynomial which depends on the operator. Plugging this expressions into the recursive relations we obtain the recursions for S_n:

$$S_{n+1}(\omega x, \bar{\omega}x, x_1, \ldots, x_{n-1}) = (\nu x + \bar{\nu}\bar{x})S_n(x, x_1, \ldots, x_{n-1})$$
$$S_{n+2}(x, -x, x_1, \ldots, x_n) = -\big(x^2\nu^2 - 1 + x^{-2}\nu^{-2}\big)S_n(x_1, \ldots, x_n) \tag{116}$$

The first few solutions are:

$$S_3 = \big(\nu^{-2}\bar{\sigma}_2 + \bar{\sigma}_1\sigma_1 + \nu^2\sigma_2\big)$$
$$S_4 = \big(\nu^{-3}\bar{\sigma}_3 + \nu^{-1}\bar{\sigma}_2\sigma_1 + \nu\bar{\sigma}_1\sigma_2 + \nu^3\sigma_3\big)$$
$$S_5 = \big(\nu^{-4}\bar{\sigma}_4 + \nu^{-2}\bar{\sigma}_3\sigma_1 + \bar{\sigma}_2\sigma_2 + \nu^2\bar{\sigma}_1\sigma_3 + \nu^4\sigma_4\big) - 1$$
$$S_6 = \big(\nu^{-5}\bar{\sigma}_5 + \nu^{-3}\bar{\sigma}_4\sigma_1 + \nu^{-1}\bar{\sigma}_3\sigma_2 + \nu\bar{\sigma}_2\sigma_3 + \nu^3\bar{\sigma}_1\sigma_4 + \nu^5\sigma_5\big) - \big(\nu^{-1}\bar{\sigma}_1 + \nu\sigma_1\big)$$
$$S_7 = \big(\nu^{-6}\bar{\sigma}_6 + \nu^{-4}\bar{\sigma}_5\sigma_1 + \nu^{-2}\bar{\sigma}_4\sigma_2 + \bar{\sigma}_3\sigma_3 + \nu^2\bar{\sigma}_2\sigma_4 + \nu^4\bar{\sigma}_1\sigma_5 + \nu^6\sigma_6\big)$$
$$- \big(\nu^{-2}\bar{\sigma}_2 + \bar{\sigma}_1\sigma_1 + \nu^2\sigma_2\big) - 1 \tag{117}$$

These suggest that S_n's are Laurent-polynomials, which are invariant under the simultaneous exchanges of $x \leftrightarrow x^{-1}$ and $\nu \leftrightarrow \nu^{-1}$. In S_n the coefficient of ν^k is a homogeneous symmetric Laurent-polynomial of degree k, for $k \in \{-n+1, -n+3, \ldots, n-1\}$. Let us define then

$$\tau_k(x_1, \ldots, x_n) = \sum_{l \in \mathbb{Z}} \nu^{2l-k}\bar{\sigma}_{k-l}(x_1, \ldots, x_n)\sigma_l(x_1, \ldots, x_n) \tag{118}$$

Here we sum over all integers l, but note that this sum is always finite. These Laurent-polynomials satisfy the following useful identities:

$$\tau_{n+1}(x_1, \ldots, x_n) = \tau_{n-1}(x_1, \ldots, x_n) \tag{119}$$
$$\tau_{k+2}(x, -x, x_1, \ldots, x_n) = \tau_{k+2}(x_1, \ldots, x_n) + \tau_{k-2}(x_1, \ldots, x_n)$$
$$- \big(x^2\nu^2 + x^{-2}\nu^{-2}\big)\tau_k(x_1, \ldots, x_n) \tag{120}$$

$$\tau_k(x, x_1, \ldots, x_n) = \left(x\nu + x^{-1}\nu^{-1}\right)\tau_{k-1}(x_1, \ldots, x_n)$$
$$+ \tau_{k-2}(x_1, \ldots, x_n) + \tau_k(x_1, \ldots, x_n) \tag{121}$$

$$\tau_{k+1}\left(x\omega, x\omega^{-1}, x_1, \ldots, x_{n-1}\right) = \left(x^{-1}\nu^{-1} + x\nu\right)\tau_k(x, x_1, \ldots, x_{n-1}) - \tau_{k-1}(x_1, \ldots, x_{n-1})$$
$$+ \tau_{k-3}(x_1, \ldots, x_{n-1}) + \tau_{k+1}(x_1, \ldots, x_{n-1}) \tag{122}$$

Using these properties it is easy to show by induction that the form factor solution is

$$S_n(x_1, \ldots, x_n) = \tau_{n-1}(x_1, \ldots, x_n) - \left(\tau_{n-5}(x_1, \ldots, x_n) + \tau_{n-7}(x_1, \ldots, x_n)\right)$$
$$+ \left(\tau_{n-11}(x_1, \ldots, x_n) + \tau_{n-13}(x_1, \ldots, x_n)\right) - \cdots$$
$$= \tau_{n-1}(x_1, \ldots, x_n)$$
$$+ \sum_{m \geqslant 1} (-1)^m \left(\tau_{n+1-6m}(x_1, \ldots, x_n) + \tau_{n-1-6m}(x_1, \ldots, x_n)\right) \tag{123}$$

The operator-dependent prefactors for φ and $\bar{\varphi}$ in (115) are

$$R^{\bar{\varphi}}(\sigma_1, \bar{\sigma}_1) = \bar{\nu}\bar{\sigma}_1; \qquad R^{\varphi}(\sigma_1, \bar{\sigma}_1) = \nu\sigma_1 \tag{124}$$

A.4. Form factors of descendant operators

Descendant operators correspond to the kernels of the recursion equations. These kernels are the same as for the bulk theory: at level n they are

$$K_n^{kin}(x_1, \ldots, x_n) = \prod_{1 \leqslant i < j \leqslant n} (x_i + x_j); \qquad K_n^{dyn}(x_1, \ldots, x_n) = \prod_{1 \leqslant i < j \leqslant n} \left(x_i^2 + x_j^2 + x_i x_j\right) \tag{125}$$

The common kernel is

$$K_n(x_1, \ldots, x_n) = K_n^{kin}(x_1, \ldots, x_n) K_n^{dyn}(x_1, \ldots, x_n) \tag{126}$$

Adding formally $K_1 = 1$ all solutions of the form factor equations originates form a top representative at level n of the form

$$\sigma_1^{a_1} \sigma_2^{a_2} \ldots \sigma_n^{a_n} K_n; \qquad a_1, \ldots, a_{n-1} \in \mathbb{N}, \ a_n \in \mathbb{Z} \tag{127}$$

but it is a highly nontrivial task to relate them to the space of local defect operators.

Appendix B. Numerical data

In this appendix we extensively present our numerical data.

B.1. Short distance expansion of the two point function

In this subsection we show the real and imaginary parts of various correlation function. The short distance CFT expansion is shown with continuous lines, while the form factor expansion with dots. In Fig. 8 we compare

$$\left\langle \Phi_-(r)\Phi_+(0)\right\rangle$$
$$\sim C^I_{\Phi_-\Phi_+} r^{4/5} + C^{\Phi_+}_{\Phi_-\Phi_+} \langle\Phi_+\rangle r^{2/5} + C^{\Phi_-}_{\Phi_-\Phi_+} \langle\Phi_-\rangle r^{2/5}$$
$$+ C^{\varphi}_{\Phi_-\Phi_+} \langle\varphi\rangle r^{3/5} + C^{\bar{\varphi}}_{\Phi_-\Phi_+} \langle\bar{\varphi}\rangle r^{3/5} \tag{128}$$
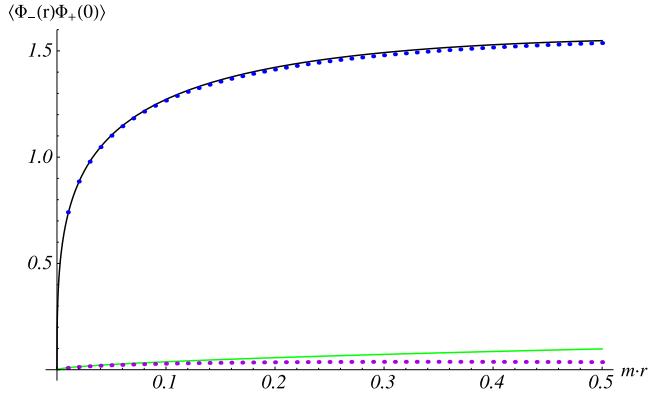
Fig. 8. $\Phi_- \Phi_+$ correlation function: blue and purple dots show the real and imaginary part calculated from the form factor expansion up to two particle terms, while black and green curves the first order CFT perturbation results. (For interpretation of the references to color in this figure legend, the reader is referred to the web version of this article.)
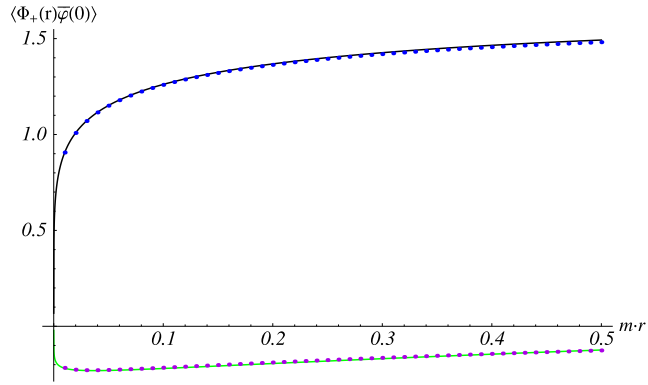

Fig. 9. $\Phi_+ \bar{\varphi} \equiv \Phi_- \varphi$ correlation function: blue and purple dots show the real and imaginary part calculated from the form factor expansion up to two particle terms, while black and green curves the first order CFT perturbation results. (For interpretation of the references to color in this figure legend, the reader is referred to the web version of this article.)

where

$$C^I_{\Phi_- \Phi_+} = \left(1 + \beta^{-2}\right), \qquad C^\varphi_{\Phi_- \Phi_+} = -i\alpha\eta^{-2}\sqrt{\sqrt{5}\left(1 + \beta^{-2}\right)},$$

$$C^{\bar{\varphi}}_{\Phi_- \Phi_+} = i\alpha\eta^2\sqrt{\sqrt{5}\left(1 + \beta^{-2}\right)}, \qquad C^{\Phi_+}_{\Phi_- \Phi_+} = C^{\Phi_-}_{\Phi_- \Phi_+} = \alpha^2/\beta.$$

Also, in Fig. 9, we present the correlator

$$\left\langle \Phi_-(r)\varphi(0) \right\rangle \sim C^{\Phi_+}_{\Phi_- \varphi}\langle \Phi_+ \rangle r^{1/5} + C^{\Phi_-}_{\Phi_- \varphi}\langle \Phi_- \rangle r^{1/5} + C^{\bar{\varphi}}_{\Phi_- \varphi}\langle \bar{\varphi} \rangle r^{2/5} \tag{129}$$

with

$$C^{\Phi_-}_{\Phi_- \varphi} = \frac{\alpha}{2}\left(\beta + \beta^{-1} - \frac{i}{\sqrt[4]{5}}\right), \qquad C^{\Phi_+}_{\Phi_- \varphi} = \frac{\alpha\beta}{2}\left(1 + \left(\beta - \beta^{-1}\right)\frac{i}{\sqrt[4]{5}}\right),$$

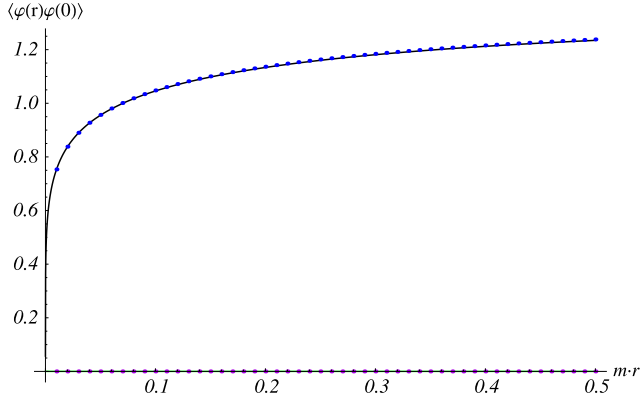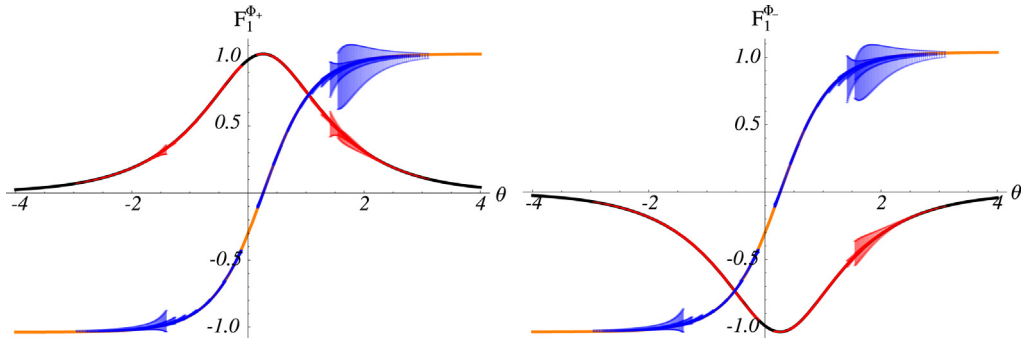$$C^{\bar{\varphi}}_{\Phi_- \varphi} = -\frac{1}{\eta\beta}.$$

Fig. 10. $\varphi\varphi$ correlation function: blue and purple dots show the real and imaginary part calculated by form factor expansion up to two particle terms, while black and green curves the first order CFT perturbation results. (For interpretation of the references to color in this figure legend, the reader is referred to the web version of this article.)

Fig. 11. Comparison between the extrapolated TCSA data (dots with confidence bars) and the theoretical prediction (solid line) for the one-particle form factor of the operators Φ_+ and Φ_-.

Fig. 10, finally, exhibits the correlation functions

$$\left\langle \varphi(r)\varphi(0)\right\rangle \sim C^I_{\varphi\varphi} r^{2/5} + C^\varphi_{\varphi\varphi}\langle\varphi\rangle r^{1/5} \qquad \left\langle \bar\varphi(r)\bar\varphi(0)\right\rangle \sim C^I_{\bar\varphi\bar\varphi} r^{2/5} + C^{\bar\varphi}_{\bar\varphi\bar\varphi}\langle\bar\varphi\rangle r^{1/5} \qquad (130)$$

where

$$C^I_{\varphi\varphi} = C^I_{\bar\varphi\bar\varphi} = -1 \quad \text{and} \quad C^\varphi_{\varphi\varphi} = C^{\bar\varphi}_{\bar\varphi\bar\varphi} = \frac{\alpha}{\beta}.$$

In all of these formulas, the vacuum expectation values of defect operators from Section 2.2.2 are used.

B.2. One particle form factors

In this subsections we present the various particle form factors. We start with the one-particle form factors of the fields $\Phi_\pm$. Data are collected from various Bethe–Yang quantization numbers and volumes (Fig. 11).

B.3. Multiparticle form factors

In this subsection we present the comparison of data for multiparticle form factors (Figs. 12, 13 and 14).
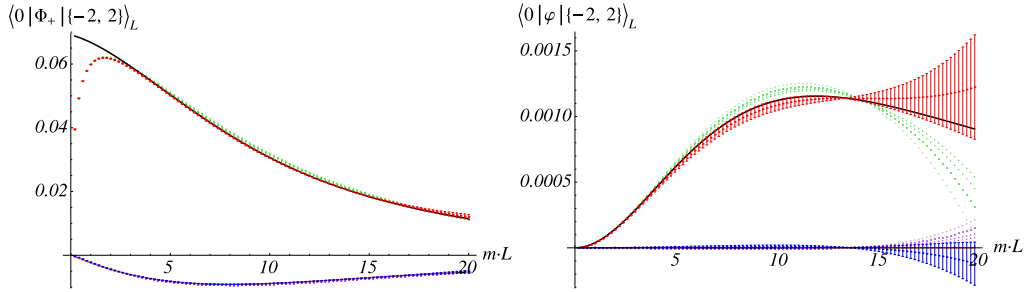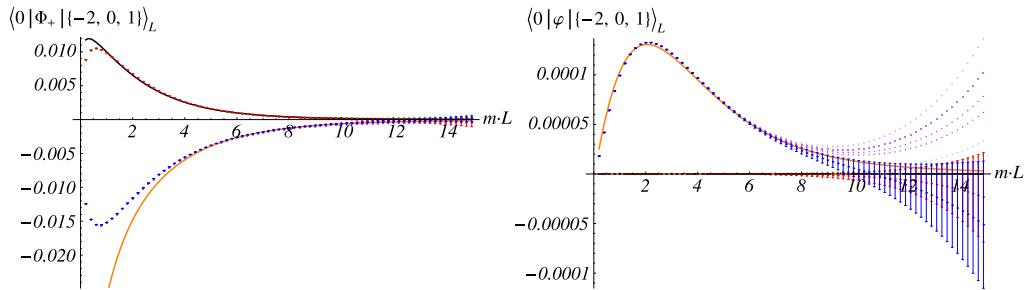

Fig. 12. Left: two-particle form factor of the operator Φ_+ on the state labeled by quantum numbers $n_1 = -2$, $n_2 = 2$. Right: two-particle form factor of the operator φ on the state $n_1 = -2$, $n_2 = 2$. The solid lines are computed from formula (72), while the dots with confidence bars are obtained by extrapolated TCSA data. (The consistent legend is described in the beginning of Section 4.1.)
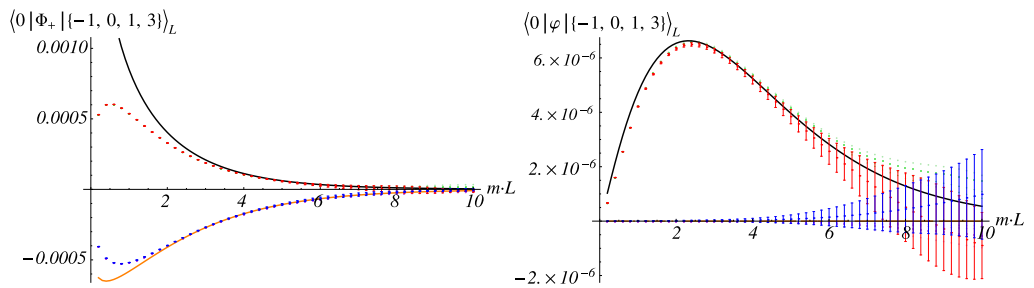

Fig. 13. Left: three-particle form factor of the operator Φ_+ on the state labeled by quantum numbers $n_1 = -2$, $n_2 = 0$, $n_3 = 1$. Right: three-particle form factor of the operator φ on the state $n_1 = -2$, $n_2 = 0$, $n_3 = 1$. The solid lines are computed from formula (72), while the dots with confidence bars are obtained by extrapolated TCSA data. (The consistent legend is described in the beginning of Section 4.1.)

Fig. 14. Left: four-particle form factor of the operator Φ_+ on the state labeled by quantum numbers $n_1 = -1$, $n_2 = 0$, $n_3 = 1$, $n_4 = 3$. Right: four-particle form factor of the operator φ on the state $n_1 = -1$, $n_2 = 0$, $n_3 = 1$, $n_4 = 3$. The solid lines are computed from formula (72), while the dots with confidence bars are obtained by extrapolated TCSA data. (The consistent legend is described in the beginning of Section 4.1.)

B.4. Diagonal form factors

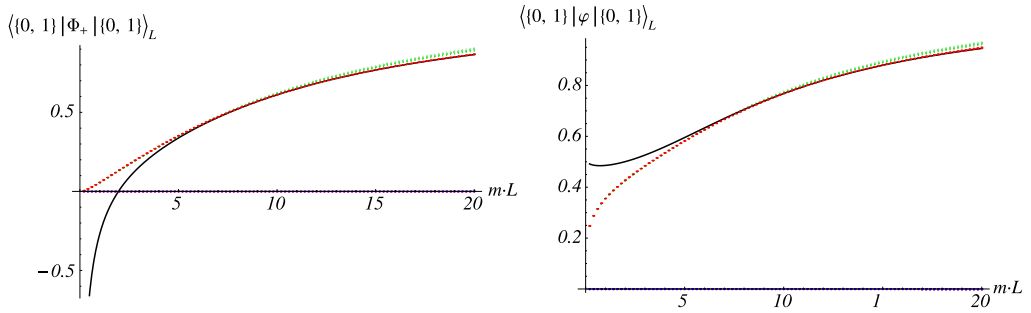This subsection contain some data for diagonal form factors with various particle numbers (Figs. 15–17).

Fig. 15. Left: two-particle diagonal form factor of the operator Φ_+ on the state labeled by quantum numbers $n_1 = 0$, $n_2 = 1$. Right: two-particle diagonal form factor of the operator φ on the state $n_1 = 0$, $n_2 = 1$. The solid lines are computed from formula (81), while the dots with confidence bars are obtained by extrapolated TCSA data. (The consistent legend is described in the beginning of Section 4.1.)
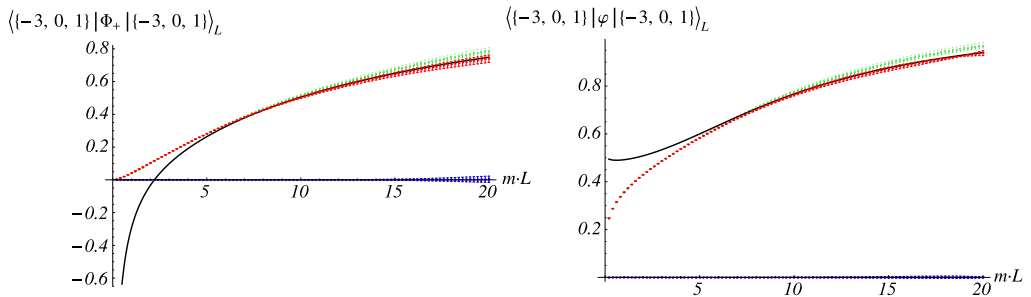

Fig. 16. Left: three-particle diagonal form factor of the operator Φ_+ on the state labeled by quantum numbers $n_1 = -3$, $n_2 = 0$, $n_3 = 1$. Right: three-particle diagonal form factor of the operator φ on the state $n_1 = -3$, $n_2 = 0$, $n_3 = 1$. The solid lines are computed from formula (81), while the dots with confidence bars are obtained by extrapolated TCSA data. (The consistent legend is described in the beginning of Section 4.1.)
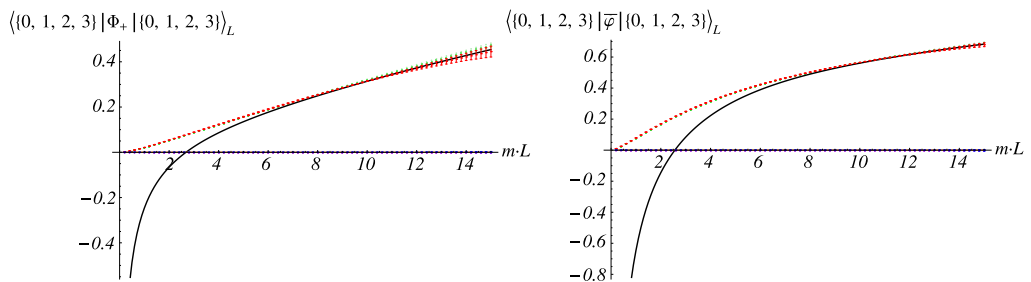

Fig. 17. Left: four-particle diagonal form factor of the operator Φ_+ on the state labeled by quantum numbers $n_1 = 0$, $n_2 = 1$, $n_3 = 2$, $n_4 = 3$. Right: four-particle diagonal form factor of the operator $\bar{\varphi}$ on the state $n_1 = 0$, $n_2 = 1$, $n_3 = 2$, $n_4 = 3$. The solid lines are computed from formula (81), while the dots with confidence bars are obtained by extrapolated TCSA data. (The consistent legend is described in the beginning of Section 4.1.)

References

[1] Jean Avan, Anastasia Doikou, The sine-Gordon model with integrable defects revisited, J. High Energy Phys. 1211 (2012) 008.
[2] Z. Bajnok, A. George, From defects to boundaries, Int. J. Mod. Phys. A 21 (2006) 1063–1078.
[3] Z. Bajnok, Zs. Simon, Solving topological defects via fusion, Nucl. Phys. B 802 (2008) 307–329.
[4] Zoltan Bajnok, Omar el Deeb, Form factors in the presence of integrable defects, Nucl. Phys. B 832 (2010) 500–519.
[5] Zoltan Bajnok, Laszlo Hollo, Gerard Watts, Defect scaling Lee–Yang model from the perturbed DCFT point of view, arXiv:1307.4536 [hep-th], July 2013.
[6] P. Bowcock, Edward Corrigan, C. Zambon, Affine Toda field theories with defects, J. High Energy Phys. 0401 (2004) 056.
[7] P. Bowcock, Edward Corrigan, C. Zambon, Some aspects of jump-defects in the quantum sine-Gordon model, J. High Energy Phys. 0508 (2005) 023.
[8] E. Corrigan, C. Zambon, Integrable defects in affine Toda field theory and infinite dimensional representations of quantum groups, Nucl. Phys. B 848 (2011) 545–577.
[9] Edward Corrigan, C. Zambon, On purely transmitting defects in affine Toda field theory, J. High Energy Phys. 0707 (2007) 001.
[10] G. Delfino, G. Mussardo, P. Simonetti, Scattering theory and correlation functions in statistical models with a line of defect, Nucl. Phys. B 432 (1994) 518–550.
[11] Anastasia Doikou, Nikos Karaiskos, Sigma models in the presence of dynamical point-like defects, Nucl. Phys. B 867 (2013) 872–886.
[12] P. Dorey, M. Pillin, R. Tateo, G.M.T. Watts, One point functions in perturbed boundary conformal field theories, Nucl. Phys. B 594 (2001) 625–659.
[13] Giovanni Feverati, Kevin Graham, Paul A. Pearce, Gabor Zs. Toth, Gerard Watts, A renormalisation group for TCSA, arXiv:hep-th/0612203, 2006.
[14] Philip Giokas, Gerard Watts, The renormalisation group for the truncated conformal space approach on the cylinder, arXiv:1106.2448 [hep-th], 2011.
[15] Robert M. Konik, Yury Adamov, A numerical renormalization group for continuum one-dimensional systems, Phys. Rev. Lett. 98 (2007) 147205.
[16] M. Kormos, G. Takacs, Boundary form-factors in finite volume, Nucl. Phys. B 803 (2008) 277–298.
[17] M. Luscher, Volume dependence of the energy spectrum in massive quantum field theories. 1. Stable particle states, Commun. Math. Phys. 104 (1986) 177.
[18] M. Luscher, Volume dependence of the energy spectrum in massive quantum field theories. 2. Scattering states, Commun. Math. Phys. 105 (1986) 153–188.
[19] Martin Luscher, Two particle states on a torus and their relation to the scattering matrix, Nucl. Phys. B 354 (1991) 531–578.
[20] L. Maiani, M. Testa, Final state interactions from Euclidean correlation functions, Phys. Lett. B 245 (1990) 585–590.
[21] B. Pozsgay, Luscher's μ-term and finite volume bootstrap principle for scattering states and form factors, Nucl. Phys. B 802 (2008) 435–457.
[22] B. Pozsgay, Form factor approach to diagonal finite volume matrix elements in integrable QFT, arXiv:1305.3373 [hep-th], 2013.
[23] B. Pozsgay, G. Takacs, Form-factors in finite volume. I. Form-factor bootstrap and truncated conformal space, Nucl. Phys. B 788 (2008) 167–208.
[24] B. Pozsgay, G. Takacs, Form factors in finite volume. II. Disconnected terms and finite temperature correlators, Nucl. Phys. B 788 (2008) 209–251.
[25] Balazs Pozsgay, Mean values of local operators in highly excited Bethe states, J. Stat. Mech. 1101 (2011) P01011.
[26] I.M. Szecsenyi, G. Takacs, G.M.T. Watts, One-point functions in finite volume/temperature: a case study, J. High Energy Phys. 1308 (2013) 094.
[27] G. Takacs, Determining matrix elements and resonance widths from finite volume: the dangerous μ-terms, J. High Energy Phys. 1111 (2011) 113.
[28] V.P. Yurov, A.B. Zamolodchikov, Truncated conformal space approach to scaling Lee–Yang model, Int. J. Mod. Phys. A 5 (1990) 3221–3246.
[29] A.B. Zamolodchikov, Thermodynamic Bethe ansatz in relativistic models: scaling three state Potts and Lee–Yang models, Nucl. Phys. B 342 (1990) 695–720.
[30] A.B. Zamolodchikov, Two point correlation function in scaling Lee–Yang model, Nucl. Phys. B 348 (1991) 619–641.